

Tutorial and Review Paper

Cite this article: Gupta P, Malviya L, Charhate SV (2019). 5G multi-element/port antenna design for wireless applications:a review. *International Journal of Microwave and Wireless Technologies* **11**, 918–938. <https://doi.org/10.1017/S1759078719000382>

Received: 15 October 2018

Revised: 11 March 2019

Accepted: 13 March 2019

First published online: 28 May 2019

Keywords:

Array; MIMO; isolation; gain; beam steering

Author for correspondence:

Leeladhar Malviya

E-mail: ldmalviya@gmail.com

5G multi-element/port antenna design for wireless applications:a review

Parul Gupta, Leeladhar Malviya and S. V. Charhate

Shri G. S. Institute of Science and Technology, Indore 452003, India

Abstract

Fifth generation (5G) is the current hot topic of the world's leading telecommunication companies. The compact designs of antennas made it possible for them to resonate at higher frequencies, thus to enable the devices to attain higher data rate as compared to 4G technology. Data rate of 5G technology for low mobility users is expected to be 50.0 Gbps and for high mobility users it is 5.0 Gbps. On the other hand, International telecommunication union's objective for 5G is 3 times more spectrally efficient than long-term evolution (LTE). The paper has carried out meticulous study over the impact of 5G antennas on the size of antenna, size/type of substrate, gain, efficiency, and isolation, etc. Also, different arrays and multiple input multiple outputs (MIMOs) with patch antenna, magneto electric-dipole, microstrip grid array antenna, folded dipole, series-fed array, connected antenna array, MIMO are studied. The paper also includes the existing technology i.e 4G LTE and their isolation enhancement approaches. Many of the designs used the reflector plates to reduce the back lobe radiation problem in MIMO/array antennas to increase front-to-back ratio. The gain in 5G antennas can be increased by using balun, parasitic element as directors, multiple notch structures, three identical slot sub-arrays, etc. Mathematical equations of multi-element/port antennas are included to model the designed antennas. The beam steering is also included for the 5G technology in this paper.

Introduction

The fourth (4G) generation technology was commercially deployed in Oslo, Norway, and Stockholm, Sweden in 2009, and since then was spread to the rest of the world. In March 2008, International telecommunication union (ITU) specified that the maximum peak speed of the technology should be 100.0 Mega bits per second (Mbps) for low mobility users like person traveling/walking on the road, and 1.0 Giga bits per second (Gbps) for high mobility users like persons traveling in car/train/aeroplane etc. The 4G technology uses frequencies in the range of 700.0, 850.0, 950.0, 1800.0, 1900.0, 2100.0, 2300.0, 2600.0, and 3500.0 MHz, etc [1, 2]. The electromagnetic field, transmission lines, and wave theory is applicable while studying the effect of different characteristics of antenna technologies [3–5].

The 4G technology was designed to work over IP packet switching network, is able to dynamically share and use the network resources to support multiple users per cell. The 4G uses scalable channel bandwidth of 5.0–20.0 MHz optionally up to 40.0 MHz and has peak spectral efficiency of 15.0 bits/s/Hz in the downlink and 6.75 bits/s/Hz in the uplink. Also, the system spectral efficiency in indoor cases is 3.0 bits/s/Hz/cell for downlink and 2.25 bits/s/Hz/cell for uplink and having smooth hand-overs across heterogeneous networks. The 4G has some other features like use of multiple input multiple output (MIMO), turbo principle error-correcting codes, channel-dependent scheduling, link adaptation to spread a boon in the market for wireless users. Major advantages of 4G technology are that it has low latency data transmission, variable data speed from 100.0 to 300.0 Mbps, has scalable bandwidth, provides uninterrupted connectivity especially for video chats and conferences, better coverage, more secure and safer than previous technologies and affordable cost effective/pricing schemes [6].

Apart from its pros, there were some cons which led scientists to switch to better technologies. Although, it offered uninterrupted connectivity, but to some regions its connectivity gets limited, and many users are annoyed by its glitches and bugs, and consume lots of battery power. Those who cannot access to 4G, have to switch to 3G/Wi-Fi while paying for the same amount as specified by 4G network plan, also users are forced to buy new devices to access 4G technology. Although, 4G long-term evolution (LTE) promised many features like serving 1 million base stations for outdoor and indoor applications, still it failed to satisfy the exponentially increasing demands of mobile and wireless users. Many researchers and mobile/wireless industries did their level best to increase data rate for most case conditions, antenna gain, etc, but failed to do so due to growing demands of the user needs [7,8].

Table 1. Spectral efficiencies of SISO and MIMO

Spectral Efficiency (bits/second/Hz)		
Technology	SISO	MIMO
4G-LTE	4.08	16.32 (4 × 4)
4G-LTE Advanced	3.75	30.0 (8 × 8)

The solution to problems of 4G is given by fifth generation (5G) technology. The 5G is built on the institute of electrical and electronics engineers (IEEE) 802.11 protocol and is aimed to speedup its data rate three times that of 4G. The mobile devices used with 4G can be modified to accommodate 5G antennas. The mobile company Xiom and Samsung are working on the world’s first 4G and 5G enabled mobile phones, which will work on 28 GHz (millimeter wave) and 3.5 GHz for 5G broadcasting, and 2.5 GHz 4G bands. Also, the 5G antenna can be assembled between LTE and wi-Fi antennas of 4G mobile phones [9–11].

The 5G technology is used by antennas with various combinations like implementing circular polarization (CP) or by forming single-user/multi-user and single-band/multi-band MIMO [12].

With the invention of wireless system, single input single output (SISO) came into the picture of growing market. It was typically less complex than MIMO as it used only one antenna in transmitter and receiver. It was used in satellite, radio, global system for mobile (GSM) communications systems. Although, it had some advantages but due to its drawbacks like high bandwidth, high interference, and range reduction in practical receivers, etc, its use is limited [13, 14].

MIMO is a more advance technology to solve the drawbacks of SISO. MIMO achieves better bit error rate (BER), delivers higher data rate due to transmission of multiple data streams/symbols, simultaneously using multiple antennas, and enhances coverage as compared to SISO. MIMO is the solution of the multipath propagation and is the vision of non-line-of-sight (NLOS) communication. MIMO also provides better results in respect of spectral efficiency, and capacity. Spectral efficiency of 4G technology is stated in table 1 for SISO and MIMO [15, 16]:

Spectral efficiency (bits/second/Hz) is calculated as per equation (1):

$$\eta = \frac{R}{B}, \tag{1}$$

where η is spectral efficiency, R is data rate, and B is bandwidth of channel.

The capacity of SISO and MIMO are formulated using equations (2) and (3), respectively:

$$C = B \log_2 \left(1 + \frac{S}{N} \right), \tag{2}$$

$$C = \log_2 \left(I_{N_r} + \frac{P}{NN_t} HH^* \right), \tag{3}$$

where I_{N_r} is identity matrix, P is signal power, N is noise power, N_t and N_r are number of transmitting and receiving antennas, H is channel matrix, and H^* is transpose of channel matrix, respectively.

The ITU passed a group of frequencies from 24.0 to 86.0 GHz for 5G technology [17]. MIMO along with 5G technology demands very high bandwidth with reduction in its size due to high frequency, and also designed on microstrip patches [18, 19]. For the 5G most of the work is concentrated on the array designs for the gain enhancement and directional radiation patterns. The generalized equation of the two element array is given as (4):

$$E_t = E_1 + E_2 = \hat{a}_{\theta} j \eta \frac{kI_0 l}{4\pi} \left\{ \frac{e^{-j[kr_1 - (\beta/2)]}}{r_1} \cos \theta_1 + \frac{e^{-j[kr_2 - (\beta/2)]}}{r_2} \cos \theta_2 \right\}, \tag{4}$$

where E_1 and E_2 are the field radiated by 1st and 2nd elements, E_t is the total field radiated by two elements, and β is the difference in phase excitation between the elements.

Above equation (4) can be modified as equation (5):

$$E_t = E_1 + E_2 = \hat{a}_{\theta} j \eta \frac{kI_0 l}{4\pi r} \cos \theta \left\{ 2 \cos \left[\frac{1}{2} (kd \cos \theta + \beta) \right] \right\}. \tag{5}$$

The total field of the array is equal to the field of a single element positioned at the origin multiplied by a factor called the array factor (AF), and is given in equation (6):

$$AF = 2 \cos \left[\frac{1}{2} (kd \cos \theta + \beta) \right]. \tag{6}$$

Similarly for N-elements AF is calculated by equation (7), and the normalized form of it is given by (8):

$$AF = \sum_{n=1}^N e^{j(n-1)(kd \cos \theta + \beta)}, \tag{7}$$

$$(AF_n) = \frac{1}{N} \left[\frac{\sin(N/2\varphi)}{\sin(1/2\varphi)} \right]. \tag{8}$$

The microstrip patch antennas are designed on various dielectric substrates like FR-4, Rogers RT Duroid, Taconic TLY-5, and polyimide, etc [20]. The general formulas of width (W), length (L), effective dielectric constant (ϵ_{reff}), variation in length (ΔL) due to fringing field, effective length (L_{eff}) of a radiating microstrip patch antenna are given by equation (9) and equation (10) [21–25]:

$$W = \frac{1}{2f_r \sqrt{\mu_0 \epsilon_0}} \sqrt{\frac{2}{\epsilon_r + 1}} = \frac{\vartheta_0}{2f_r} \sqrt{\frac{2}{\epsilon_r + 1}}, \tag{9}$$

$$L = \frac{1}{2f_r \sqrt{\epsilon_{reff}} \sqrt{\mu_0 \epsilon_0}} - 2\Delta L, \tag{10}$$

where f_r is resonant frequency, μ_0 and ϵ_0 are the permeability and permittivity of free space, ϵ_r is relative dielectric constant, ϑ_0 is the free-space velocity of light.

The ϵ_{reff} , ΔL and L_{eff} are calculated by equations (11),(12), and (13), respectively:

$$\epsilon_{\text{reff}} = \frac{\epsilon_r + 1}{2} + \frac{\epsilon_r - 1}{2} \left[1 + 12 \frac{h}{W} \right]^{-1/2}, \tag{11}$$

$$\Delta L = 0.142h \frac{(\epsilon_{\text{reff}} + 0.3)(W/h + 0.264)}{(\epsilon_{\text{reff}} - 0.258)(W/h + 0.8)}, \tag{12}$$

$$L_{\text{eff}} = L + 2\Delta L. \tag{13}$$

Mode of microstrip patch antenna can be determined by using the formula (14):

$$f_{m,n,p} = \frac{1}{2\pi\sqrt{\mu_r}} \sqrt{\left(\frac{m\pi}{h}\right)^2 + \left(\frac{n\pi}{L}\right)^2 + \left(\frac{p\pi}{W}\right)^2}, \tag{14}$$

where, m , n , and p are variables to find the desired mode, and h is the height of the substrate.

The return loss (RL) in case of a single antenna/MIMO is given by equation (15):

$$RL(\text{dB}) = 10 \log_{10} \frac{1}{\rho^2}, \tag{15}$$

where ρ is the reflection coefficient.

The characterization of multi-port/element or MIMO antennas for the diversity performance is done in terms of envelope correlation coefficient (ECC), mean effective gain (MEG), and total active reflection coefficient (TARC). The formulas of ECC (ρ), and MEG are given by (16), (17), and (18), respectively [26]:

$$|\rho(i, j, N)| = \frac{\left| \sum_{n=1}^N S_{i,n}^* S_{n,j} \right|}{\sqrt{\left| \prod_{k(=ij)} [1 - \sum_{n=1}^N S_{i,n}^* S_{n,k}] \right|}}, \tag{16}$$

$$MEG_1 = 0.5 \eta_{1,\text{rad}} = 0.5[1 - |S_{11}|^2 - |S_{12}|^2], \tag{17}$$

$$MEG_2 = 0.5 \eta_{2,\text{rad}} = 0.5[1 - |S_{12}|^2 - |S_{22}|^2], \tag{18}$$

where S_{11} and S_{22} are reflection coefficients at ports 1 and 2, S_{12} is port isolation, MEG_1 and MEG_2 are due to port 1 and 2 (in case of two ports only and is a generalized equation).

The another formulas of the MEGs are given by (19), and (20), respectively:

$$MEG_j = \oint \left(\frac{XPR}{1 + XPR} P_{\theta_j(\Omega)} G_{\theta_j(\Omega)} + \frac{1}{1 + XPR} P_{\phi_j(\Omega)} G_{\phi_j(\Omega)} \right), \tag{19}$$

$$MEG_j = \frac{1}{2\pi} \int_0^{2\pi} \left[\frac{XPR}{1 + XPR} G_{\theta_j}\left(\frac{\pi}{2}, \phi\right) + \frac{1}{1 + XPR} G_{\phi_j}\left(\frac{\pi}{2}, \phi\right) \right] d\phi, \tag{20}$$

where XPR is the cross-polarization ratio. The value of XPR equals 0 dB for outdoor environment, and XPR equals 6.0 dB for indoor environment, respectively, and $G_{(\theta j)}$ and $G_{(\phi j)}$ are the gain parameters in azimuthal and elevation planes, respectively.

Similarly, TARC (Γ_a^t) includes the effect of random variables and excitation angles at different ports of a designed multi-port antenna. TARC can be calculated for the designed multi-element/port or MIMO antennas using the equation given as (21):

$$\Gamma_a^t = \frac{\sqrt{|(S_{ii} + S_{ij} * e^{jq})|^2 + |(S_{ji} + S_{jj} * e^{jq})|^2}}{\sqrt{N}}, \tag{21}$$

where θ is input phase angle, S_{ii} and S_{ij} are the input reflection coefficient and isolation between the ports, respectively.

The ECC, MEG, and TARC parameters for multi-port/element antenna can be obtained in terms of all the scattering parameters as well in terms of far-field characteristics. The ECC is an alternative to isolation parameter between any two ports or among all the ports of a designed antenna. The MEG is used to find the suitability of designed antenna under different environments e.g. isotropic, Gaussian etc, for indoor and outdoor applications. The TARC is used to find the active bandwidth and phase angles of the signals applied to the various ports. TARC curve resembles the shape of returnloss or isolation parameter for a particular combination of phase relations at ports.

Isolation enhancement techniques

Multi-port/element or MIMO antennas are designed in a compact space due to the requirement of the compact, portable, and wireless devices. This compactness may create the mutual coupling among the radiating elements of the designed antennas [27]. Various approaches like neutralization line [28, 29], defected ground structure (DGS) [30], inverted L-branches and slots [31–34], T-shaped metallic/slotted isolator [35–38], circular isolator [39], split ring resonator (SRR) [40], ground modification techniques like partially extended ground (PEG) [41] and partially stepped ground (PSG) [42], cross-dipoles with baluns [43], and radio frequency choke (RFC) as band stop [44] are used to control the degrading effects of mutual coupling.

MIMO is also affected by the back lobe radiations due to the slotting in the ground. To solve the problem of back lobe radiation, a reflector plate is used behind the ground plane [45]. MIMO antenna with a reflector achieves high isolation, low cross polarization, high front-to-back ratio (FBR), and low side lobes [46]. The enhancement of FBR can also be done by feeding both identical antenna elements with equal magnitude current having 90° phase difference [47].

MIMO antennas with space diversity, pattern diversity, and polarization diversity are used with monopoles/dipoles to control the effect of mutual coupling [48–56]. The polarization diversity also controls the space required in MIMO implementation.

There are linearly polarized and circularly polarized (CP) SISO/MIMO antenna designed for stationary and moving users. The CP can be obtained using magneto electric (ME) dipole antenna [57], rectangular slots apart by 90° etched at the center of a truncated rectangular patch, and also by diagonal feeding [58].

MIMO with mathematically inspired generalized shape [59], MIMO with proximity coupled rings for capacitive effect [60], MIMO with semi-printed structure and fractals [61], hybrid

MIMO antenna with arrow-shaped monopole and a bended dipole with gap-coupled feed and L-shaped strips [62], multi-layer MIMO [63], multiband MIMO [64] is a system of multi-element antennas like array antennas [65]. Similarly, the narrowband and wideband antennas are designed for various applications.

MIMO with rectangular dielectric resonator antenna (RDRA) [66], aperture coupled cylindrical dielectric resonator (ACCDRA), cylindrical DRAs (CDRAs) with metallic reflector are used to increase isolation [67], and are also used for multiband operation [68]. Some equations of the DRA are given by (22), (23), and (24) [69]:

$$f_r = \frac{6.321c}{2\pi\sqrt{\epsilon_{r,eff} + 2}} \left[0.21 + 0.36 \left(\frac{r}{2H_{eff}} \right) + 0.02 \left(\frac{r}{2H_{eff}} \right)^2 \right], \quad (22)$$

where c is velocity of light, $\epsilon_{r,eff}$ is effective dielectric constant, r is radius of CDRA, and H_{eff} is effective height of antenna. The $\epsilon_{r,eff}$ and H_{eff} are obtained as:

$$\epsilon_{r,eff} = \frac{H_{eff}}{H/\epsilon_{Alumina} + H_s/\epsilon_{sub}}, \quad (23)$$

$$H_{eff} = H + H_s, \quad (24)$$

where H and H_s are the height of CDRA and substrate, respectively.

5G antenna designs

Various designs of 5G SISO/MIMO/array antennas [70] are described as follows in this section.

The lower spectrum of 5G bands is covered under the 3.3–4.2 GHz and 4.4–4.99 GHz. The higher frequency spectrum for 5G band covers frequencies like 24.25–27.5 GHz, 26.5–27.5 GHz, 26.5–29.5 GHz, 27.5–28.28 GHz, 27.5–28.35 GHz, 37.0–40.0 GHz, and 37.0–43.5 GHz which are deployed in countries like China, Korea, Japan, etc. Frequencies above 60.0 GHz are 53.3–66.5 GHz, 55.4–66.6 GHz, 56.6–64.8 GHz, 57.0–64.0 GHz and 57.0–65.0 GHz.

5G which is promising to deliver upto 1000 times as much data as today's networks, will also consume upto 1000 times as much energy as now. This consumption is becoming a hot topic to concern about. 5G small cell base stations are proposed to consume more than 50% of energy and can approach upto 800 watt with massive MIMO for high volume traffic. Hence, computation of power can play a vital role in energy efficiency of small cell networks. As computation power increases with the heavy traffic, transmission power reduces. Thus, there is a trade-off between these two. On comparing these two, former is small compared to latter, therefore, the energy efficiency investigation of small cell networks focuses on the optimization of transmission power at base station (BS). In this technology, power can be saved by BS sleeping scheme, where the RF's and transmitters of BS are closed during no traffic. As the number of antennas and bandwidths are increased, computation power also increases. Thus in 5G, computation power will play a more important role than transmission power, therefore both the powers should be

considered while optimizing energy efficiency in 5G small cell networks [71].

Variety of dielectric substrates are available to design 5G antennas. While selecting the dielectric substrate material, its properties must be checked e.g. amount of surface wave production, loss tangent, permittivity, dispersion constant, anisotropy property, aging effect, temperature range, humidity effects, weight, elastic constant, solderability, mechanical strength, conformability, and cost etc [72].

The Polyethylene Terephthalate (PET) is commonly available polyester resin and also used in fibers. It is a nanocomposite in emerging applications. Its dielectric constant at 10.0 GHz is 3.2, dissipation factor is 0.002, surface resistivity is 10^{13} Ohm/cm², and volume resistivity is $>10^{14}$ Ohm-cm [73]. The Polydimethylsiloxane (PDMS) is a very flexible siloxane (Silicone) and most popular polymer. Its dielectric constant at 10.0 GHz is 2.7, dissipation factor is 0.0012, surface resistivity is 10^{14} Ohm/cm², and volume resistivity is $>10^{15}$ Ohm-cm. These materials are the dielectric materials for the 5G and emerging antenna technologies. The PET and PDMS offer low value of dielectric constants when combined with other materials like glass microsphere (GM) [74].

Microstrip patch antenna was fabricated and designed on polyethylene terephthalate (PET) of thickness 0.125 mm to cover X-band for 5G technology. The modified coplanar waveguide (CPW) feed with curtailed corners of patch were used to widen the bandwidth of the X-band region. The dimension of antenna was 60.0 × 75.0 mm². The gain of 5.0 dBi and 38.0% efficiency was obtained in the frequency band of 7.0–13.0 GHz. The design is shown in Fig. 1 [75].

When an array has a stacked structure of two shared aperture having sub-arrays orthogonally polarized, then it achieves wide bandwidth and stable gain in all the bands. Each pair of driven patches shared two parasitic patches by which the antenna achieves compactness. The slits and DGS are used to enhance the isolation. Rogers RO 4350 substrate with multiple layers were used with thicknesses of 0.762, 0.508, and 1.27 mm, respectively. The size of the antenna was 77.0 × 79.0 × 2.2 mm³. The different polarizations are achieved with the X-band as X-band horizontal (XH) and X-band vertical (XV); and with the Ku-band horizontal (KuH) and Ku-band vertical (KuV). The frequencies achieved in XH band is 8.3–11.3 GHz, in XV band is 8.7–11.5 GHz, in KuH band is 12.2–15.5 GHz, and in KuV band is 13.0–15.2 GHz, respectively. The horizontal and vertical components of polarizations in X-band have minimum of 200 MHz change in lower and upper frequencies. Similarly, the horizontal and vertical components of polarizations in Ku-band have minimum of 300 MHz change in lower and upper frequencies. The gain in XH band is 14.1 dB, in XV band 13.2 dB, in KuH band is 12.7 dB, and in KuV band is 12.7 dB, respectively. The isolation was >20.0 dB in all the bands. The design is shown in Fig. 2 [76].

Substrate integrated waveguide (SIW) corrugated structures were used to design antennas instead of using waveguide feeder and grooves on a metallic plate. To analyze performance characteristics, antenna was made up of two and four grooves separately. At the bottom layer, transmission line was used to feed the antenna and in the middle layer, power was coupled to the patch. By employing grooves, high gain and narrow radiation patterns were achieved. For two groove antenna, gain was 11.3 dBi and for four grooves it was 12.8 dBi. Overall efficiency yielded >84.0% in the band. The frequency band for two grooves was

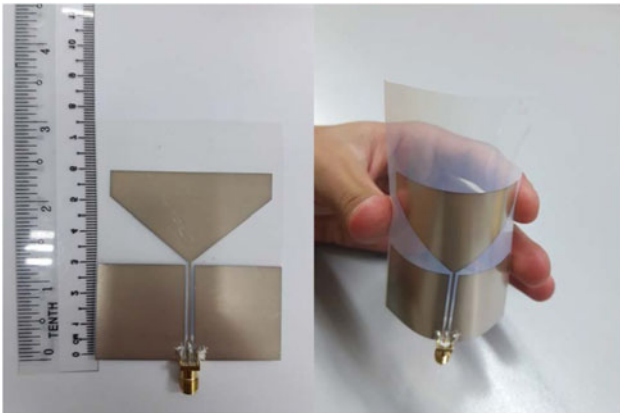


Fig. 1. Microstrip patch antenna with PET substrate ©[75]

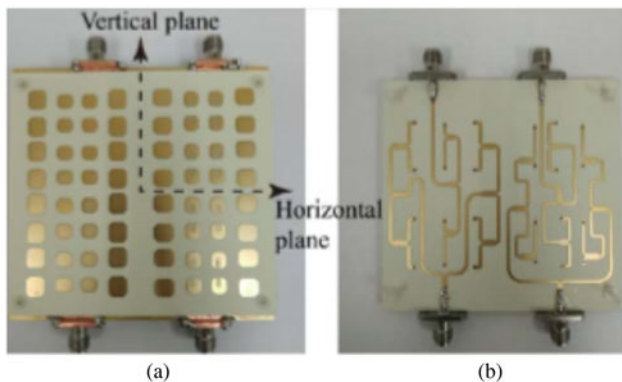


Fig. 2. Antenna array (a) Array structure (b) Feed networks ©[76]

10.02–10.65 GHz while for four grooves, it was 10.09–10.7 GHz. Rogers 4003 having height of 0.508 mm was used for first and third substrates, while Rogers TMM4 having height of 3.175 mm was used for second substrate [77].

A flexible microstrip grid array antenna (MGAA) was inherited to design 5G antennas because of its ability to operate at high frequency and obtaining high gain. MGAA was designed using 1.9 mm thick polydimethylsiloxane (PDMS) substrate, while patch and ground plane were designed using conductive rubber material. MGAA consisted of 17 rectangular mesh cells having 24 radiating elements, thus enabling gain of 11.2 dBi at 15.5 GHz. The designed antenna covered the frequency range of 12.0–18.0 GHz. The total dimension of antenna was $60.0 \times 2.4 \text{ cm}^3$ [78].

To utilize the device-to-device (D2D) communication, gain was increased in DRA array by steering the beam from -32° to $+32^\circ$, achieving wide frequency range from 13.0 to 17.0 GHz. The resonant frequency was 15.0 GHz. The TE_{163}^y mode DR was applied as driven element having narrow aperture in the ground plane to connect shorting pins. The DR having ECCOSTOCK HiK material was attached to ground plane using double sided duct tape having 0.058 mm thickness. The feeding network was fabricated on Duroid 5880 having thickness of 0.254 mm. The overall size of the antenna was $30.0 \times 20.0 \text{ mm}^2$. The achieved bandwidth was more than 1.3 GHz. The design is shown in Fig. 3 [79].

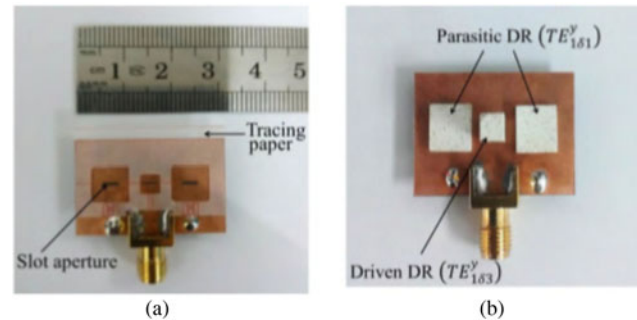


Fig. 3. (a) Without DR (b) With DR ©[79]

An antenna was made with a total of 16 rectangular meshes having short and long sides. The longer side acted as a transmission line but shorter side acted as a radiating element. If the length of the shorter side decreases below 9.84 mm, reflection coefficient increases. The FR-4 substrate having $49.0 \times 58.0 \times 1.6 \text{ mm}^3$ size was used to design the compact grid array antenna for 13.8–15.9 GHz frequency range. At 15.9 GHz, gain and efficiency were marked as 14.4 dBi and 66.0%, respectively. The design is shown in Fig. 4 [80].

To investigate power density of antenna at two operating frequencies i.e. at 15.0 and 28.0 GHz, two uniform linear patch arrays were used having 8×1 elements with a distance of $\lambda/2$ between them. On top of the phone chassis of dimension $140.0 \times 78.0 \text{ mm}^2$, an antenna array was mounted along with plastic box. Each patch element was $4.6 \times 5.7 \text{ mm}^2$ and $3.1 \times 4.0 \text{ mm}^2$ at 15.0 and 28.0 GHz, respectively. The design achieved more than 15.0 dB of isolation for both arrays. Two types of substrates were used in the design. The first substrate was Rogers 4003 for 15.0 GHz, and second substrate was Rogers 5800 for 28.0 GHz with thickness of 0.8 mm [81].

Three identical sub-arrays of patch antennas were placed on the different sides of the antenna to attain 3D broad scanning coverage. Desired directions of beam were obtained by switching feeding to one of the 3 sub-arrays. Thus, a gain of higher than 10.0 dB was obtained in the frequency range of 21.0–22.0 GHz. A 1×8 linear array antenna was used, where each element was excited by equal magnitude. The center-to-center distance between each element was $\lambda/2$, having λ as the wavelength of 21.5 GHz. Total and radiation efficiencies were $>80.0\%$ and $>95.0\%$, respectively. The Nelco N9000 substrate of thickness 0.787 mm was in the design, and the overall dimension of antenna was $110.0 \times 55.0 \times 4.5 \text{ mm}^3$ [82].

A compact 8-element tapered slot antenna (TSA) was designed on Rogers RT 5880 covering 21.0–23.0 GHz frequency band. These elements were placed on the top portion of mobile's PCB to form an array. An antenna fed by hockey-stick balun, was designed to resonate at 22.0 GHz. The size of the antenna was $6.0 \times 12.0 \text{ mm}^2$, yielding the gain above 20.0 dB and efficiency of $>95.0\%$ [83].

To increase the performance of an antenna, the resonator of conventional slot antenna was converted to air-filled slot loop structure. The narrow slot was made by a large copper metal surface having length equal to half guided waveguide and width equal to small fraction of λ . Thus, a metal ring resonator and a cubic slot were designed to nullify the sensitivity characteristics of the designed antenna. In 21.0–23.5 GHz frequency, gain was

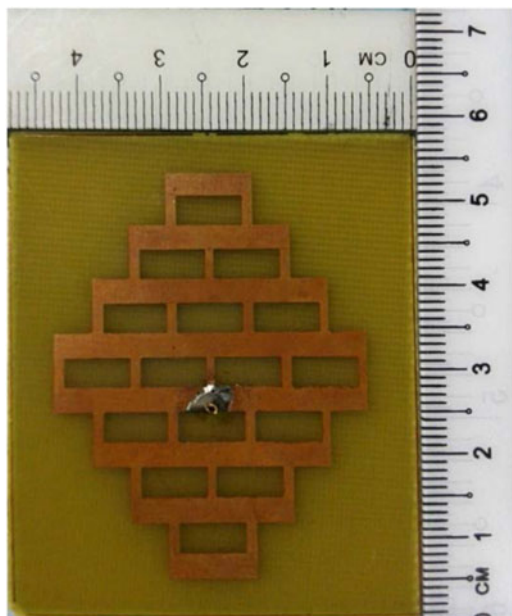


Fig. 4. Antenna with 16 rectangular meshes ©[80]

>5.5 dBi, while efficiency was >90.0%. The size of the FR-4 substrate was $10.0 \times 5.0 \times 0.8 \text{ cm}^3$ [84].

Two 4×4 array elements were implemented on the board, consisting of two stacked substrates. Top of upper substrate consisted of patch. Top and bottom of lower one consisted of U-shaped slot and micro-pin resonator plus hair-pin, respectively. The height of antenna and substrate were <1 and 0.2 mm (lower), and 0.787 mm (upper), respectively, whereas RO 4003C (lower) and RO 5880 (upper) were used as the type of substrates. The frequency range of the antenna array was 22.0–32.0 GHz with a gain of 19.0 dBi in the band. The design is shown in Fig. 5. The dimensions of U-slot and hair-pin resonators were obtained using the equations (25) and (26) [85]:

$$L_{u1} + 2 * L_{u2} \approx \frac{c}{2f_o \sqrt{\epsilon_{eff1}}}, \quad (25)$$

$$L_{r1} + 2 * L_{r2} \approx \frac{c}{2f_o \sqrt{\epsilon_{eff2}}}, \quad (26)$$

where L_{u1} , L_{u2} , L_{r1} , and L_{r2} are the dimensions of the U-slot and hair-pin resonators, respectively, f_o is the resonant frequency, ϵ_{eff1} and ϵ_{eff2} are the effective dielectric constants, and c is the speed of light.

A $1/2$ wavelength antenna element array achieved good beam-forming performance in H -plane. Millimeter-wave (MMW) circuit integrated substrate waveguide feeds the antenna element. The frequency band of 22.5–32.0 GHz having VSWR <1.45 and gain between 8.2 and 9.6 dBi were achieved in the design [86].

A wideband microstrip comb-line linear array antenna which worked in millimetre wave was operated over 28.0 GHz frequency and was made with Taconic TLY-5 substrate. The antenna consisted of 12 elements, reflection canceling slit structure, stubs, matching element and a via hole. Substrate's thickness and relative permittivity were 0.508 mm and 2.2, respectively. The design provides bandwidth from 27.5 to 29.5 GHz with sidelobe levels

in the range of only 6.167%. The distance between the elements is 4.076 mm. The stub matching is used to enhance the performance and impedance bandwidth of the antenna. The design is shown in Fig. 6. The length of the radiating element was found to be 3.38 mm using the following equation (27) [87]:

$$E_L = \frac{c}{2f_r \sqrt{\epsilon_{re}}} - 2\Delta E_L, \quad (27)$$

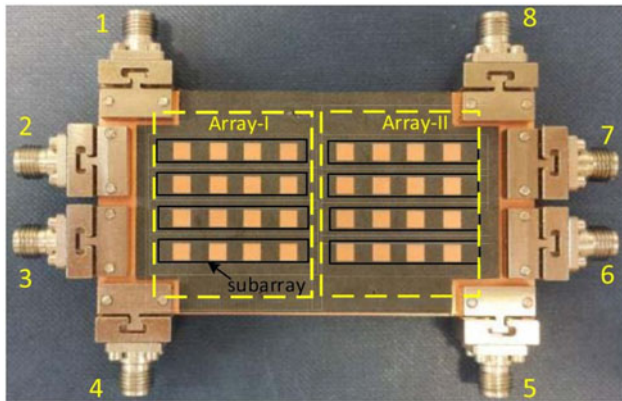
where ΔE_L is the fringing field, f_r is resonant frequency, ϵ_{re} is effective relative permittivity and c is speed of light.

A single dipole, 2×1 arrays, and 4×1 arrays were implemented and polarized vertically to achieve high gain, high radiation efficiency, wide bandwidth, and low cross-polarization. The gain of the combination was increased using parasitic element in-front of dipole as directors, while half power beam-width (HPBW) was increased by implementing directors as V-shaped. The via fence suppressed back-radiation, enhancing FBR by surrounding the dipole structure. Thus, by covering range of 24.0–32.0 GHz, dipole antenna, 2×1 and 4×1 arrays achieved a gain of 7.13, 9.83, and 12.61 dBi, respectively. The dimensions of electric dipole, 2×1 array, and 4×1 array were $10.0 \times 24.2 \times 4.9 \text{ mm}^3$, $15.0 \times 26.47 \times 4.9 \text{ mm}^3$, and $30.0 \times 35.62 \times 49.0 \text{ mm}^3$, respectively. Rogers RO 5880 was used to fabricate electric dipole antenna having efficiency of 95.8%. The design is shown in Fig. 7 [88].

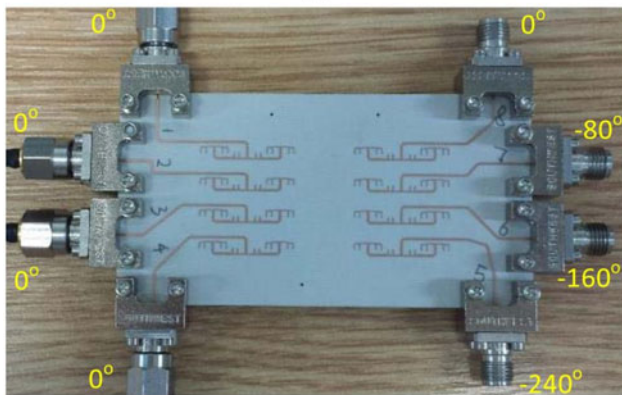
To reduce mutual coupling and enhancing isolation between the elements of 5G antipodal vivaldi antenna (AVA) array, 1×8 power dividers were used to feed the elements. On ground plane, multiple notch structures were added so that the isolation increases between them. Thus, an enhancement isolation, shift in frequency band from 24.65–28.5 GHz to 24.55–28.5 GHz, and enhancement in gain from 6.93 to 11.32 dB were achieved. The size of the antenna was $28.82 \times 60.0 \times 0.787 \text{ mm}^3$ on Rogers 5880 substrate having thickness of 0.787 mm. The design is shown in Fig. 8 [89].

A design was realized using three identical slot sub-arrays which controlled surface waves in order to have 3D coverage beam scan. Each sub-array had 8 elements separated with distance of 6.75 and 2.25 mm, respectively. The size of the antenna and substrate were $4.85 \times 0.5 \text{ mm}^2$ and $65.0 \times 130.0 \times 0.764 \text{ mm}^3$, respectively. The Nelco N9000 PCB having relative permittivity of 2.2 and loss tangent of 0.0009 was used for substrate. The 25.0–30.0 GHz of frequency band was covered with isolation level of more than 12.75 dB, gain of 18.52 dBi, and ECC of <0.07 between two arrays. Total efficiencies of the three sub-arrays were 74.3, 68.0, and 72.2%, respectively [90].

A printed dipole angled at 45° was fed by an integrated balun which consisted of a 50 ohm microstrip line and a rectangular slot. An 8-element linear array was implemented to increase the beam-forming of antenna. The feed line was placed on top of substrate while dipole and ground plane on the back. Balun was used to match the impedance over broad frequency range, as it acted as microstrip-to-slot line transformer. The gain obtained by single antenna lied between 4.5 and 5.8 dBi and bandwidth of 36.2% in the frequency band of 26.5–38.2 GHz. While the antenna array achieved gain of 11.5–12.5 dBi and frequency band between 25.0 and 38.0 GHz. The arrays were fed by 8 ports. Mutual coupling was decreased by inserting microstrip stub between two printed dipoles with distance of 4.8 mm from center-to-center spacing. The antenna was fabricated on Rogers RT/Duroid 5880 substrate having thickness of 0.254 mm. The efficiency of >93.0% was achieved in the band [91].



(a)



(b)

Fig. 5. Prototype of two arrays ©[85]



(a)



(b)

Fig. 6. Comb-line array antenna ©[87]

As 5G cellular network needs high bandwidth with low compact size and low design complexity, therefore DGS can be used for designing of 5G antennas. In this design, top surface of antenna consisted of radiating patch element with coplanar waveguide (CPW)-fed with T-shape, and the bottom part contained DGS having two iterations of symmetrical split ring slots. The isolation was enhanced by increasing distance between two adjacent

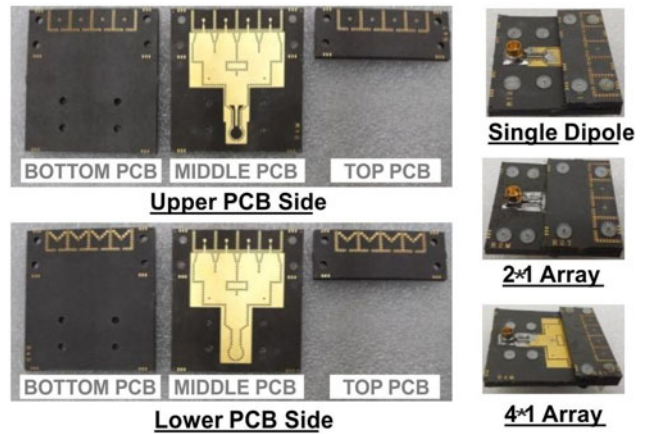


Fig. 7. Electric dipole antennas ©[88]

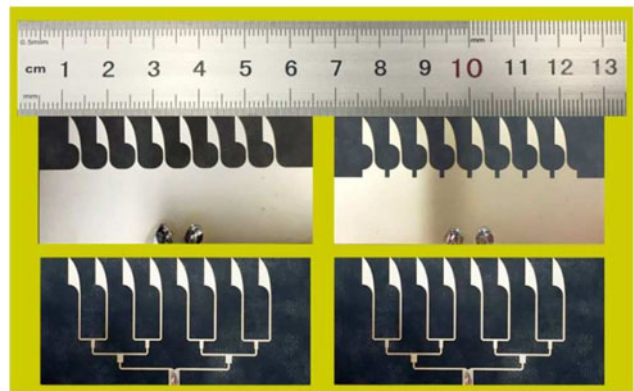


Fig. 8. AVA array without coupling and with coupling reduced ©[89]

patch elements. The size of a single antenna was $12.0 \times 12.0 \text{ mm}^2$ on Rogers RT Duroid 5880 substrate having thickness of 0.8 mm. In the 25.1–37.5 GHz frequency band, ECC was <0.09 . The gain was 10.6 dBi at 36.0 GHz and more than 80.0% efficiency in the band. The design is shown in Fig. 9 [92].

In order to have advantages like low profile, wide bandwidth and high radiation efficiency, frequency selective surface (FSS) superstrate was selected to have high dense dielectric patch antenna instead of metallic patch. The antenna was fed by aperture-coupled technique. Thus, by employing FSS, gain of 17.78 dBi at 28.0 GHz and radiation efficiency of 90.0% were obtained. The frequency band of 26.0–30.5 GHz was obtained by placing 7×7 unit cells on the two sides of substrate. The square dense dielectric (DD) patch antenna, excited by coupling slot was placed above FSS layer. Rogers RT/Duroid 6002 (loss tangent = 0.0009) was used to print DD patch, while bottom substrate was of Rogers RT 3010 (loss tangent = 0.023) material. Both substrates were 0.508 mm thick. The overall dimension of antenna was $32.0 \times 32.0 \times 1.8 \text{ mm}^3$. The design is shown in Fig. 10 [93].

The Antenna-in-Package (AiP) design consisted of multilayer organic building substrates was designed to support both horizontal and vertical polarizations. The size of the antenna and substrate were $2.0 \times 2.0 \text{ mm}^2$ and $20.0 \times 20.0 \text{ mm}^2$, respectively, whereas organic build-up was used as a substrate. The covered

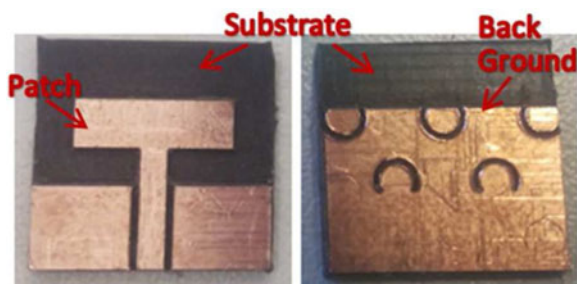


Fig. 9. MMW antenna with DGS ©[92]

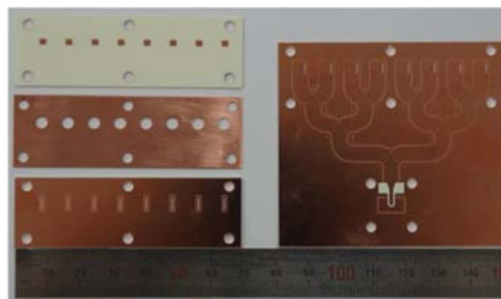


Fig. 11. 8-element antenna structure ©[97]

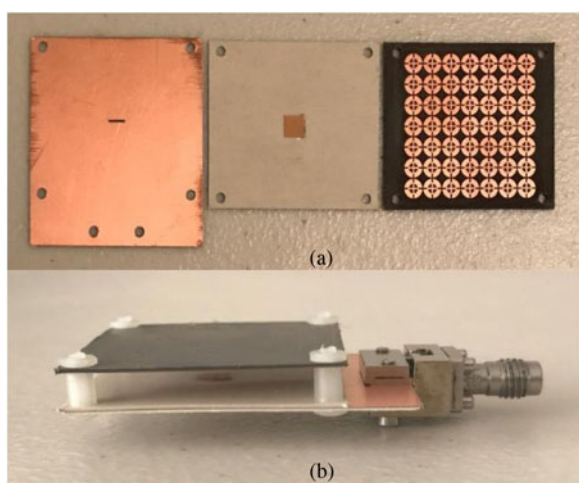


Fig. 10. Array antenna (a) Front, middle, and back (b) antenna prototype ©[93]

frequency range was 26.0–36.0 GHz. At 30.5 GHz frequency, gain was 3.8 dBi [94].

For enabling device-to-device communication in 5G network, a CP antenna was operated at 28.0 GHz frequency [95]. The obtained frequency band was in the range of 27.5–28.35 GHz for 5G cellular network. An omnidirectional circularly polarized (OCP) antenna offered high gain, larger radiation coverage, and diverse communication links. Overlapped impedance bandwidth and 3 dB axial ratio bandwidth covered 2.2 GHz from 26.5 to 28.7 GHz. The height of antenna was 1.0 mm. At the center frequency of 27.6 GHz, gain was 0.7 dB. The dimension of substrate was 19.71 mm² [96].

An antenna array having ground plane half of the size of Samsung Galaxy Note 4 was designed by stacking three substrates and a copper plate. To obtain broadband performance, an 8-way SIW feeding network based on Taylor distribution with broadband 4-stage unequal T-junction dividers plus cavity-backed antenna were designed to analyze its performance. On the upper side of substrate-1, antenna array was placed having 8 longitudinal slots to transmit wave from 1 to 2. This transmission of wave was done by coupling apertures of substrate-1 mounted on substrate-2 for the same purpose. Coupling apertures, cavity holes in Cu plate and radiating patches all constituted an 8-element cavity backed aperture-coupled antenna array. The gain of 14.9 dBi and efficiency of 75.0% were obtained in the frequency band of 26.5–29.7 GHz. The 0.508 mm thick Rogers 4350 B was used to fabricate the antenna. The design is shown in Fig. 11 [97].

A proximity coupled linear array antenna yielded a gain of over 13.5 dB by covering a frequency band of 26.5–28.92 GHz. The increase in bandwidth was due to linear manner of coupling from the feedlines above the substrate to the patches on the upper substrate and back down to the next feedline below and onwards. Both the substrates were made up of Taconic TLY-5 having thickness of 0.508 mm. The design is shown in Fig. 12. The number of elements were calculated as follows (28) [98]:

$$D = dir + 10\log(N), \quad (28)$$

where D is the directivity of the array, dir is the directivity of the single element, and N is number of elements in the array.

An antenna was designed on the concept of SIW slots. The antenna consisted of two SIW grooves and SIW slots which reduce mutual coupling in MIMO antenna. The SIW slot does not need any extra layer as required by SIW slit. The two MIMO antennas were designed to compare the performances based on the design parameters. MIMO 1 has dimension of 72.0 × 17.2 mm² with a SIW groove, whereas MIMO 2 has 39.8 × 33.4 mm² with SIW groove almost doubled than MIMO 1. The thickness of Rogers 5880 substrate was 1.575 mm. The gain of MIMO 1 was 9.5 dBi, whereas that of MIMO 2 was 11.0 dBi. An isolation level of higher than 20.0 dB, while ECC of lower than 0.02 were achieved for both MIMO antennas in the frequency band of 26.8–28.4 GHz [99].

Two Taconic TLY-5 substrates of thickness 0.508 mm were used for antenna having center frequency of 28.0 GHz. The lower substrate had 50 ohm microstrip line feeder which feeds the patch on the upper substrate. The length of feed varied directly with spacing between the patches and inversely with size of patches and with width of feedlines. The design achieved gain of 21.0 dBi over the frequency band of 26.9–29.21 GHz. The design is shown in Fig. 13 [100].

To attain left-hand and right-hand CP, two types of antenna elements were used. Each of the elements consisted of 4 layers, having substrate 1, 2, copper plate and substrate 3. A slot was etched in substrate 1 so that wave can transmit from 1 to 2. Similarly, slot of same dimension and location was etched in substrate 2. The circular drilling was done in copper plate and lastly on substrate 3. The desired CP can be obtained with a circular radiating patch. The antenna was printed on the Rogers 4350 B having 0.508 mm thickness. The size of single antenna was 70.0 × 63.5 × 2.2 mm³. It covered 3 frequency bands namely 26.9–30.9 GHz, 27.1–29.95 GHz, and 26.55–29.65 GHz. The 13.09 and 13.52 dBi gains were obtained for left-hand circularly polarized (LHCP) and right-hand circularly polarized (RHCP) modes, respectively. The design is shown in Fig. 14 [101].

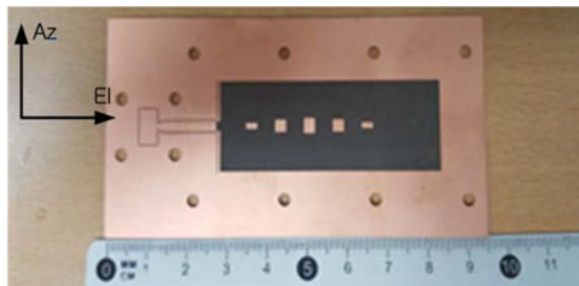


Fig. 12. Proximity coupled linear array antenna ©[98]

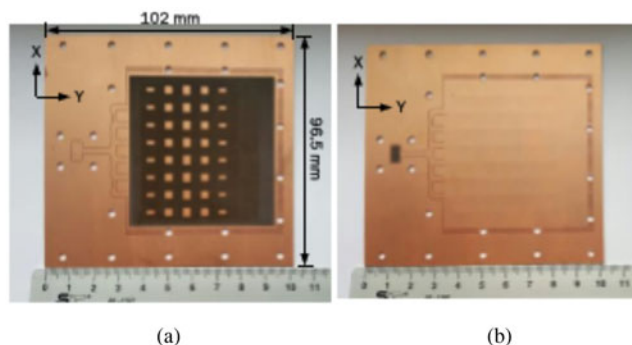


Fig. 13. Linear array antenna (a) front view (b) back view ©[100]

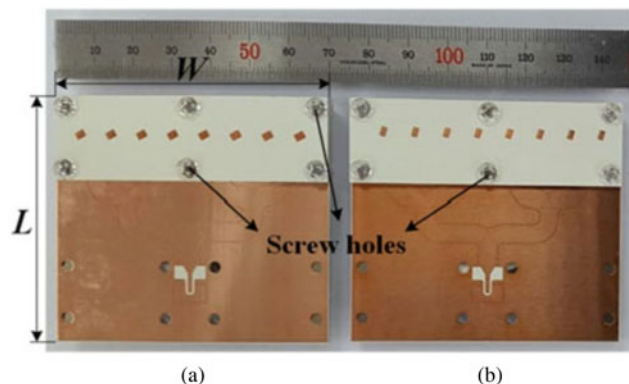


Fig. 14. Antenna array (a)LHCP and (b)RHCP ©[101]

By using concept of traditional Wilkinson power divider, an antenna was modified to change the output power division ratio continuously. This power divider was used to feed the antenna to form a beam. To ensure flatness of power division, 2-varactor loaded L-shaped open stubs were connected to two branch lines of the device. Matching at different divisions were done by using two asymmetrically coupled lines at the output port and a stepped-impedance transformer at the input port. The Rogers RT/Duroid 5880 with 0.127 mm thickness was used as a substrate. The isolation was >10.0 dB over a frequency band of 27.0–29.0 GHz [102].

The RDRA antenna fabricated on RT/Duroid 5880 was fed by microstrip line in order to provide proper matching and ease in

fabrication. As the number of elements increases, gain also increases but size of the antenna decreases. The gain of the antenna and array are calculated by equations (29) and (30), respectively:

$$G = \eta * D, \quad (29)$$

$$G = n * E_o * AF, \quad (30)$$

where G is the gain of antenna, E is radiated electrical field, E_o is electrical field produced at center array by single DRA, n is number of elements, and AF is array factor.

To compensate between size and gain, 4 elements were used in the array. The spacing between the elements was 0.78λ to increase the gain while having acceptable side lobe level. The isolation in the frequency range of 27.0–29.1 GHz was obtained above 15.0 dB, while gain of 12.1 dB fulfilled the requirement of 5G application. The dimension of substrate was $11.0 \times 12.0 \times 0.254 \text{ mm}^3$. The design is shown in Fig. 15 [103].

To compare the characteristics of metallic patch antenna and to enhance its performance, antenna was made with dense dielectric (DD) patch for 5G network. This DD PCB is easily compatible with radio frequency/microwave circuitry. The antenna comprised of two substrates. Four circular shaped DD patch radiators fed by 1-to-4 Wilkinson power divider were surrounded by electromagnetic bandgap (EBG) structure. The frequency band covered the range of 27.0–32.0 GHz, while gain and efficiency in the band were 16.3 dBi and 71.8%. The size of the RT 5880 substrate was $20.0 \times 20.0 \times 5.35 \text{ mm}^3$ with thickness of 0.508 mm. The design is shown in Fig. 16 [104].

In a cascode low noise amplifier (LNA), an inductor placed between common gate and source, was replaced by DGS because it reduces the overall silicon substrate area leading to overall reduction in the antenna size. It also provided good internal matching condition. Inductive and capacitive effects were easily attained in the antenna by implementing two rectangular slots of appropriate dimensions. Both of the rectangular slots were connected with the help of a small slot/gap. The inductive effect increased with the increase in current path, while capacitive effect increased because of charge accumulation in the slot. The peak-to-peak gain was obtained as 20.0 dB. The CMOS having thickness of 130.0 nm was used to fabricate antenna of dimension 0.27 mm^2 for 27.2–29.0 GHz frequency application. The capacitance and inductance of DGS structure were calculated by equations (31) and (32) [105]:

$$C_{DGS} = \frac{w_c}{Z_o * g_1} \cdot \frac{1}{w_o^2 - w_c^2}, \quad (31)$$

and

$$L_{DGS} = \frac{1}{w_o^2 C_{DGS}}, \quad (32)$$

where w_c and w_o are the 3.0 dB cut-off and resonant angular frequencies, Z_o is the characteristic impedance and g_1 is normalized one-pole parameter of butterworth low-pass filter. The design is shown in Fig. 17.

A 16 cavity-backed slot antenna was designed on the back case of mobile. On left and right sides, two element phased arrays were

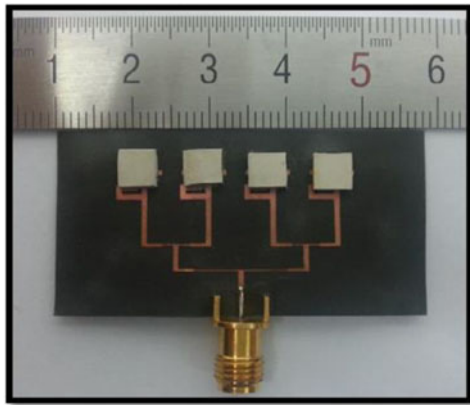


Fig. 15. Linear array DRA ©[103]

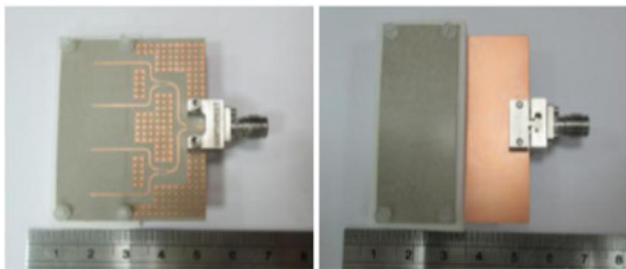


Fig. 16. DD patch array antenna ©[104]

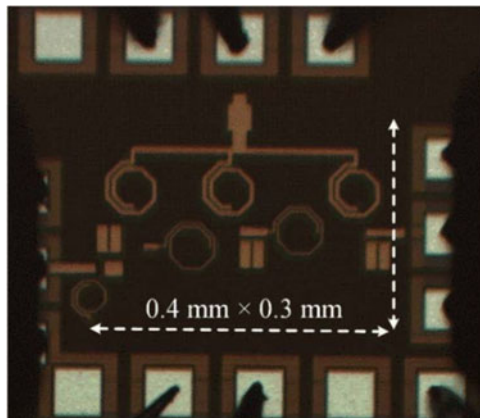


Fig. 17. Die micro graph of LNA ©[105]

built i.e on left and right sides of mobile casing for beam steering at broadside. The size of the antenna and Rogers 5880 substrate were $5.8 \times 1.5 \text{ mm}^2$. The thickness of substrate was 0.254 mm. The gain in the frequency band of 27.5–30 GHz was 6.9 dBi, and isolation level was more than 17.0 dB across the band of interest [106].

The 2×2 and 3×3 series-fed patch antennas were designed with connected patches to have high-impedance microstrip lines. Two types of designs were implemented, the first design

with one phase shifter resulted in good radiation and impedance characteristics, while the second design threw light upon ways to decrease number of ports. The Rogers RT/Duroid 5880 of thickness 0.25 mm was used to design 27.61–28.43 GHz frequency band antenna, having gain of 7.73 dB, efficiency of 88.0%, and isolation level of >29.0 dB. The designed antenna resonates at 28.0 GHz frequency. The design is shown in Fig. 18 [107].

A 28.0 GHz switched five beam antenna consisted of rectangular waveguide and reconfigurable semiconductor circuit (RSC) was designed with slots which could be opened/closed with the help of switch pin to achieve desired configuration. The RSC was attached with WR28 waveguide to compose reconfigurable radiating structures (RRSs). These RRS structures formed 3 beams which were directed towards 0° , 30° , and 45° . The gain of each beam was similar because of the opening of a different number of slots in odd number i.e 3, 5, 9 which produced beams in 0° , 30° , and 45° , respectively. High-current operational amplifiers were used to control antenna's aperture. In the frequency band of 27.9–28.5 GHz, antenna yielded gain of >6.0 dBi [108].

A 1×4 antenna array was designed to resonate at 28.0 GHz and covered a band of 22.0–35.0 GHz, uses a U-shaped thin lens designed by phase shifting filter. This lens was placed at a distance of 5.0 mm from the antenna array, whose dimension was $4.1 \times 30.6 \times 8.3 \text{ mm}^3$. A single element in array consisted of 1 driven element and 2 parasitic directors. The driven element contained one top and bottom patch plates separated by FR-4 substrate. The top patch plate was connected to feedline whereas bottom one to ground. Similarly, directors have top and bottom plates, connected through shorting vias. The gain was >3.8 dB and efficiency was 43.0%. The size of the antenna was $24.7 \times 20.8 \times 0.8 \text{ mm}^3$ on Rogers 6010 substrate having thickness of 0.25 mm [109].

A radial line slot array antenna (RSA) designed to cover frequency band of 27.0–29.0 GHz (resonating at 28.0 GHz) consisted of 2 parallel plates. The upper plate contained radiated slot patterns, while lower plate acted as a ground. The patterns were cut in circular dimension on top of the board and the air was filled between ground and RT Duroid 5880 substrate. The gain was 23.3 dB and efficiency was 96.0% at resonate frequency. The size of the antenna was 78.0 cm^2 on RT Duroid 5880 substrate [110].

To reduce mutual coupling, DGS was applied which included 12 unit cells arranged in a special manner, below the feeding line. Each unit cell contained two opposed C-shaped slot configurations used for concentrating magnetic and electric fields. Thus, a 4×4 microstrip patch array antenna was designed having three radial patches with tapering towards outer end. In the frequency band of 28.0–38.0 GHz, gain was more than 17.61 dB and efficiency was more than 92.2%, respectively. The size of Rogers Duroid RT 5880 substrate was $50.0 \times 50.0 \times 0.508 \text{ mm}^3$. The design is shown in Fig. 19 [111].

An array was designed on Franklin array concept in order to obtain multiple frequency bands instead of single one. The non-radiating stubs turned into folded-dipole antennas and radiating patches shared a phase shift of 180° . Therefore, the antenna consisted of rectangular patch and a stub, both radiating at different frequencies. The gain was achieved as 13.5 dBi with 70.0% efficiency in the 37.0–39.0 GHz frequency band. The thickness of Rogers RT/Duroid substrate was 0.8 mm. The design is shown in Fig. 20 [112].

CP achieves good 3D beam-steering characteristics, and this was showed with the help of an antenna having 12 dual-band

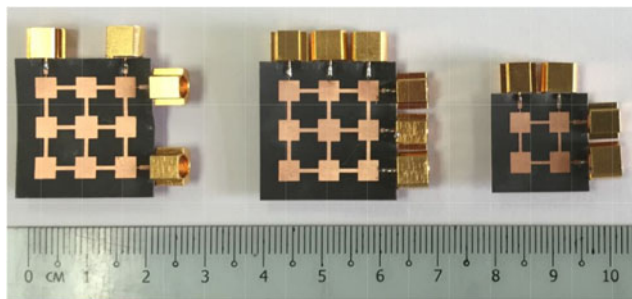


Fig. 18. 2×2 and 3×3 series-fed array antennas ©[107]

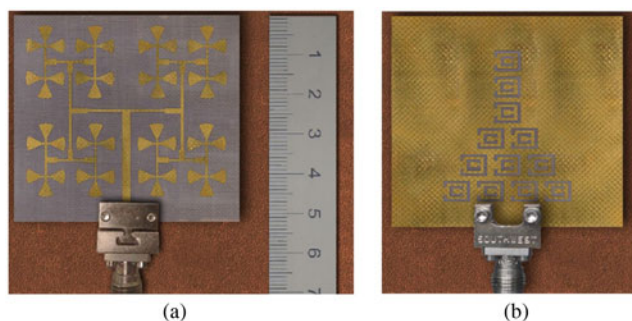


Fig. 19. 12 unit cell array antenna (a) Front view (b) Back view ©[111]

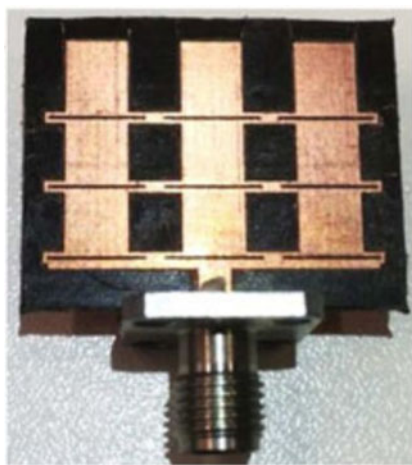


Fig. 20. Franklin array concept-based antenna ©[112]

CP antenna elements, which formed linear array in the edges of mobile phone. In this way, reflection coefficient of less than -15.0 dB, more than 7.68 dB gain, more than 15.0 dB isolation, more than 64.75% efficiency, and <3.0 dB AR values were achieved in the 28.0 – 38.0 GHz frequency band. The size of 0.8 mm thick N9000 PTFE substrates were $110.0 \times 55.0 \times 1.6$ mm³ [113].

An antenna was placed in front of a wideband lens to increase the gain. The four substrates namely RT 3003, RT 6002, and RT 5870 were used to form multi-layer antenna. The height of substrates were 0.765 , 0.5 , and 0.254 mm, respectively. The antenna was excited by a tilted slot having a CP ME-dipole. The lens

consisted of three layers of mu-near zero (MNZ) unit cells and each layer consisted of 3×4 dual-polarized low index meta-material unit cells. In the frequency range of 31.0 – 35.0 GHz, the gain was >10.0 dBi, while efficiency was $>94.0\%$ [114].

A 1×4 array antenna with tapered line feeding technique was designed to achieve 12.0 dB for mobile applications. The distance of 4.0 mm was present between the adjacent elements. Thus, for 5G communication, microstrip patch antenna was used to resonant at 38.0 and 54.0 GHz frequencies with 1.94 and 2.0 GHz bandwidths in each band respectively. The size of the antenna and Rogers RT 5880 substrate were $6.0 \times 6.25 \times 0.578$ mm³ and $6.0 \times 6.25 \times 0.508$ mm³, respectively. The gains of 6.9 and 7.4 dBi were achieved for 38.0 and 54.0 GHz frequencies [115].

To enhance gain in 5G mobile antenna a bow-tie parasitic cell was developed, which includes several bow-tie directors and parasitic patches. Bow-tie directors were based on quasi-yagi principle. The patches enhanced antenna gain by increasing transverse radiation aperture of antenna. Rogers 5880 substrate of thickness 0.508 mm was used to design the antenna for 40.0 – 50.0 GHz frequency band, having gain between 7.3 and 12.5 dBi [116].

A 2×2 sub-array antenna was formed using complementary sources, having two dipoles on the opposite sides of slot and surrounded by a cavity. Using the above design, 4×4 and 8×8 large antennas have been developed. The frequency band covered a range of 50.0 – 74.0 GHz i.e. for 4×4 array it is 57.0 – 71.0 GHz and for 8×8 it is 56.1 – 70.6 GHz. Also for 4×4 array, gain and efficiency were 21.5 dBi and 90.0% , respectively, and for 8×8 array, it is 26.7 dBi and 80.0% , respectively. The overall gain of antenna was 8.7 dBi. The antenna dimensions of $44.4 \times 14.4 \times 2.5$ mm³ for 4×4 array and $28.8 \times 28.8 \times 2.5$ mm³ for 8×8 array were utilized on Rogers 5880 substrate having 0.787 mm thickness. The design is shown in Fig. 21[117].

For operation in short range having high-data rate under 60.0 GHz wireless personnel area network (WPAN) systems, an antenna was designed having edge-coupled parasitic patch structure and a rotational feeding network. The designed antenna was used to obtain broad impedance bandwidth via dual resonance. The first resonance occurred due to circular patch antenna at 59.0 GHz, while second resonant was due to parasitic patch radiator occurred at 64.5 GHz. The gain of >12.0 dBi was obtained in the frequency range of 53.3 – 66.5 GHz. Taconic RF-30 substrate having $18.0 \times 18.0 \times 0.254$ mm³ dimension was used to design the antenna. The design is shown in Fig. 22 [118].

An antenna was designed having a combination of fabry-perot cavity (FPC) and printed ridge gap waveguide techniques to improve the radiation performances. By placing dual-layer partially reflective surface (PRS) above a slot antenna, FPC was formed. This square slot controls the bandwidth and also adds degree of freedom. To feed the antenna, PRGW technology was used to excite the rectangular slot antenna on the Rogers RT 5880 material. The circular patches connected to ground plane acted as EBG and were printed on Rogers 3003 material of thickness 0.5 mm. Thus a dual-layer unit cell made of Rogers RT 5880 material of thickness 0.254 mm was designed to construct PRS to operate at 60.0 GHz. The efficiency of better than 90.0% and gain of 16.8 dB were achieved in the frequency range of 55.4 – 66.6 GHz. The antenna dimension was 14.8×18 mm² [119].

A meta-surface sandwiched between two DRAs was arranged in H -plane to increase isolation. This meta-surface was constructed of split ring resonator (SRR) which functions as band-stop filter over 60.0 GHz frequency range. The conductive

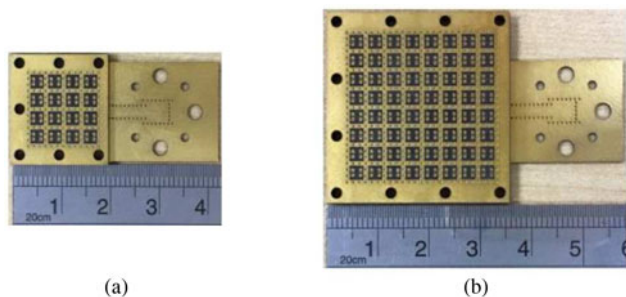


Fig. 21. Antenna arrays (a) 4×4 (b) 8×8 ©[117]

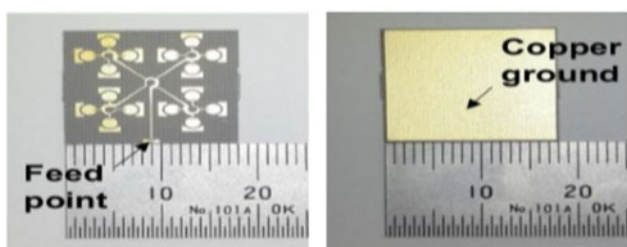


Fig. 22. 60.0 GHz WPAN antenna array ©[118]

elements of SRR acted as conductive material and the gap in ring as capacitive material. The SRR was fabricated on top and bottom of RT 5880 material having thickness of 0.254 mm, while DR and rectangular slot on the upper side of substrate. Lower substrate fabricated with RT 6010 having thickness 0.254 mm consisted of feedlines to excite DRA through rectangular slot cut out of upper substrate. Thus 1×2 DRAs having 1×7 SRR array was designed to cover 56.6–64.8 GHz frequency range yielding 7.9 dBi gain and 91.0% efficiency. By loading DRA with 1×7 array of unit cells, the obtained isolation was 46.5 dB [120].

The three antenna arrays, each having 16 patch elements were fabricated on top of RT/Duroid 5880 substrate material having height of 0.127 mm. Each of them were placed parallelly in 4 rows and 4 columns. On the bottom layer, DC lines for switch control were placed where the ground plane was also present. The achieved gain by first, second, and third arrays were 18.7, 18.6, and 18.8 dB, respectively. The frequency band covered a range of 57.0–63.0 GHz. The size of the antenna was $31.0 \times 46.4 \text{ mm}^2$. The design is shown in Fig. 23 [121].

Multi-sin-shaped corrugated antipodal fermi-tapered slot antenna (MSC-AFTSA) array was designed in which multi-corrugated patterns were implemented. The antenna consisted of grooved spherical lens (GS-lens). The three element wide scan profile AFTSA was fed to the spherical lens which orientated a wide angular coverage for transmission and receiver. The MSC was used to increase the optimization process. Together, they decreased side-lobes, enhanced radiation characteristics and impedance matching. The size of the antenna was $44.2 \times 51.6 \times 25.4 \text{ mm}^3$ on RO 4003 substrate. The thickness of substrate was 20.0 mm. The gain and efficiency were 20.0 dB and 83.0%, respectively in the frequency band of 57.0–64.0 GHz [122].

A 4×4 multi-beam antenna array, generating 16 beams was designed using aperture-coupled ME-dipole antennas. The stacking of five Rogers 5880 substrates of thickness 0.787 were

used, where vertical inter-connections were realized using substrate 1 to 3 while horizontal interconnection through 4 and 5 substrates. The gain yielded between 10.0 and 14.7 dBi and efficiency between 35.0 and 40.0% in the frequency range of 57.0–64.0 GHz. Antenna's total dimension was $5.0 \text{ mm} \times 5.0 \text{ mm}$ [123].

Similarly, two planar antennas were designed for 60.0 GHz spectrum, where, each one consisted of a 2×2 array covering 2 channels. The first antenna achieved maximum gain in point-to-point link over maximum distance of 10.0 m, while the other one was used in point-to-multipoint applications to achieve maximum beam-width. The range of frequency band was 57.0–65.0 GHz. RT Duroid 5880 substrate was used with 10.0 mil thickness. The size of the first antenna with 13.2 dBi gain was 0.25 cm^2 , and that of the second one with 10.3 dBi was 0.16 cm^2 . The design is shown in Fig. 24 [124].

A CP antipodal curvedly tapered slot antenna (CP-ACTSA) array was designed, which was fed by substrate-integrated waveguide. Rogers 6002 substrate having thickness 0.762 mm was filled with two different rectangular waveguides. The waveguide having wider section consisted of two symmetrical, antipodal and exponential tapered slots. This waveguide was fabricated by wire cutting electrical discharge machine. The slots further consisted of two curves. Thus, the CP antenna array was able to cover 5G upper E-band i.e from 81.0 to 86.0 GHz and 5G upper W-band i.e from 92.0 to 95.0 GHz. The size of the antenna was $9.55 \times 12.0 \text{ mm}^2$, with 19.88 dBic gain and 80.6% efficiency [125].

Beam steering techniques and transceiver

The beam steering is a challenge for 5G antennas. Most of the work is carried out on beam steering with 5G array antennas. Beam steerable is the process of controlling interference in terms of channeling far-field radiation pattern in a particular direction where high path loss, signal attenuation, and misalignment due to heavy air flow are prevalent. The beam steering is the ability of millimeter wave and an essential part of communication and Radar. In the past, most of the beam steering techniques were utilized, but at the expense of antenna only. The different techniques to steer the radiation pattern of an antenna are: Beamforming, Mechanical (based on MEMS switches), Reflectarray (Reflector and array), Integrated lens antenna (ILA), Switched beam antenna (antennas are arranged to cover the particular angle), Retrodirective antenna (to redirect radiation towards origin), Traveling wave antenna, Parasitic steering, and Metamaterial antenna-based [126].

In a two array system, first array was fed with the currents in quadrature with the other array to obtain the desired far field radiation pattern. Thus, by controlling the amplitude of each array, beam steering is achieved [127]. In a design, electronically steerable beam was produced by altering the parasitic element and using simple switching and tracking circuitry. The same design utilized the active element, and the parasitic element was placed at a position between open and short circuits to reduce induced current. This in turn controls the radiation losses [128]. A combination of electrically and mechanically beam steering uses the monopole and parasitic elements to make frequency dependent far field radiation performance. An impedance matching network is utilized to feed the antenna and parasitic elements [129].

The modern phase shifter monitors the phase difference between the closest radiator and microcontroller and then controls the phase shifter for the desired beam using miniaturized

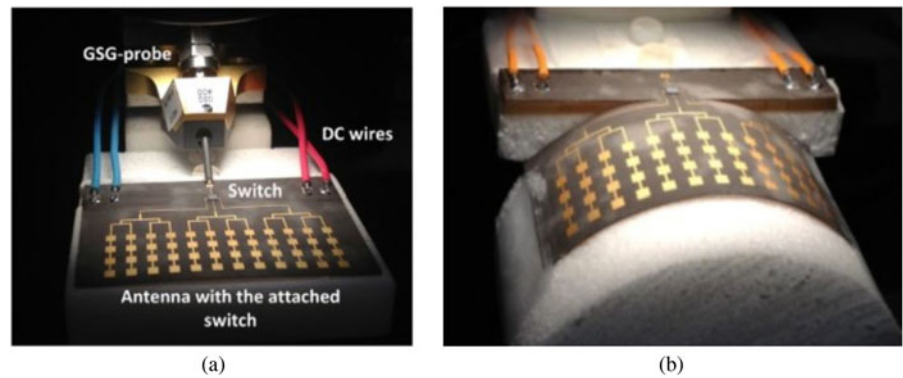


Fig. 23. Array antenna (a) Planar prototype (b) Convex prototype ©[121]

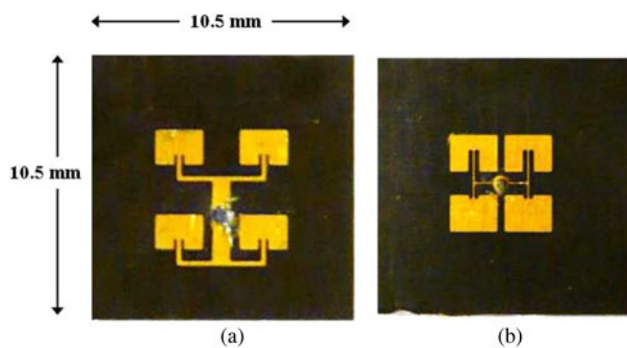


Fig. 24. 2×2 array antenna for 60.0 GHz spectrum ©[124]

antenna arrays [130]. A design uses a combination of oscillators and phase locked loops (PLL) to steer the beam by switching array antenna using a single control voltage. The beam scanning range is the function of frequency of the PLL. The beam positioning error can be controlled, to produce sum and difference radiation patterns using double pole-double throw switch and difference amplifier. By the use of prescalers, $\pm 90^\circ$ beam scanning extension can be achieved. The configuration of antenna array with coupled phase locked loop is given in Fig. 25 [131].

The modified beam steering can combine the cassegrain antenna structure, where main reflector and sub-reflector are used. The sub-reflector due to light weight and rotational nature is able to steer beam, whereas, phase of the array is controlled by proper feeding. The design was utilized for satellite communication [132].

At 28 GHz 2×3 and 2×4 arrays with single phase shifter on each port was utilized with unequal amplitude application. Hence, number of radiating elements were minimized. The approach produced better impedance matching, better radiation beam, and reduction in side/back lobe levels [133].

Along with the beam steering techniques, there is a beamforming technique also for the Massive MIMO technology for the next generation of 5G applications to reduce the intra- and inter-cell interference problems [134].

In an adaptive beam steering system, switched beam system is adapted to get desired radiation characteristics, and then beam steering is achieved by I and Q signal components. In this technique, phased local oscillator is used to adjust phase and weight of antenna element. Such method is used in steerable

massive array to independently generate beams for 5G communication [135].

A CP switched beam array was designed using 90° branch line couplers, 45° phase shifters, and patched array [136]. The CP provides line-of-sight communication and reduces multipath effects. The butler matrix with CP antenna array provides the desired rotation in beam within the scanning area in the range of 5.98–6.11 GHz with peak gain of 7.8 dB. The switched beam antenna with 4×4 butler matrix is given in Fig. 26 [137].

A 28 GHz CMOS transceiver was designed with 2×4 patch antenna array for 5G application. The design achieved good beam control arrangement and better RF performance parameters. The construction of the transceiver is explained in detailed here. The radio system consisting of 8-channel transceiver array is interfaced with digital front-end (DFE) to process baseband signals. The P-I-N diode switches are used since time division duplex (TDD) mode is used for operation. On the front end, 8-commercial 9-W power amplifiers (PA) along with 8 LNA are used that yields gain of 19 dB. Each pair of PA (LNA) is preceded by phase-shifter component giving an 11.25° phase resolution. Wilkinson power divider/combiner network is located between the RF front-end and the pre-amplifiers in 2×2 configuration. Operating frequency is regulated by serial peripheral interface (SPI) bus while phase shifters by shift registers via second SPI bus. A pumped gallium arsenide (GaAs) mixer containing integrated LO amplifier between intermediate frequency (IF) and final RF is used as up and down converter. Receiver path contains commercial logarithmic detector that works on IF frequency and is situated behind directional couplers. Finally, the antenna array is connected to the coupler for desired beam steering to achieve. The corresponding transceiver is given in Fig. 27 [138].

THz technology

As our technology is getting advanced day-by-day and so are its uses, we are in need of such a set of frequencies which will fulfill all our requirements and demands, which was not earlier by lower frequencies. Tera-hertz (THz) technology will meet the growing demands in the field of medical, astronomical, sensing, defence, communication, etc. The one THz or 10^{12} Hz is a set of frequencies between infrared and microwave frequency bands. The reason of this growing demand of THz technology is because of its capability to penetrate high with low attenuation loss, non-ionizing nature, high-resolution imaging power, etc. The THz frequency

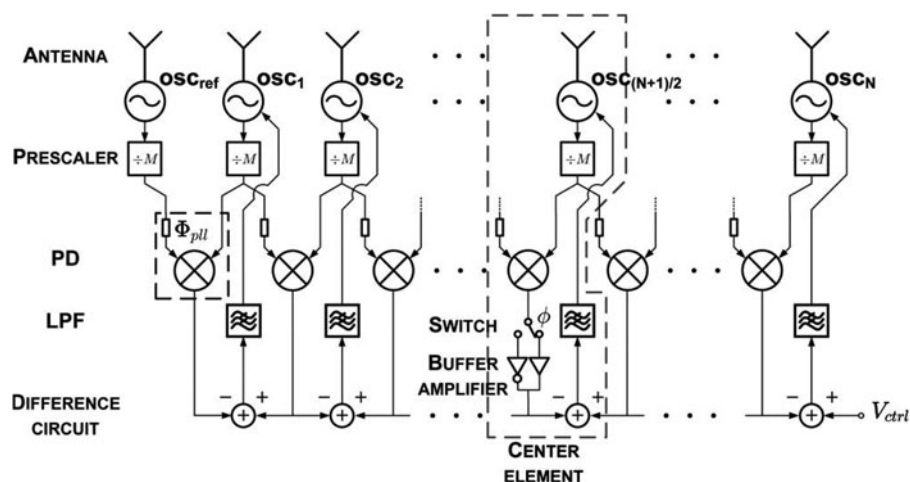


Fig. 25. Configuration of antenna array with coupled phase locked loop array ©[131]

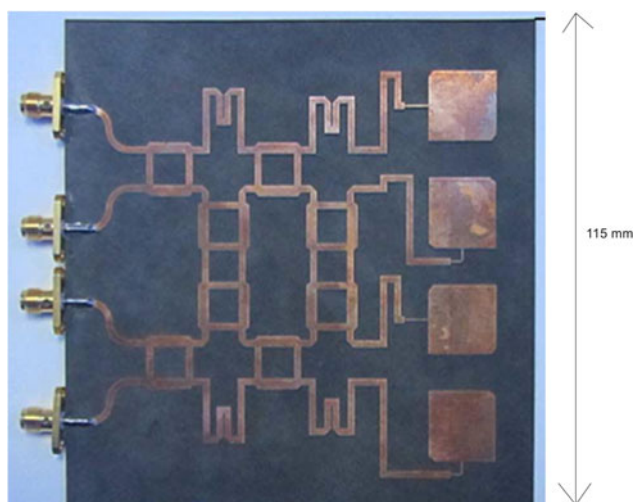


Fig. 26. Switched beam array antenna using butler matrix ©[137]

spectrum is aimed to work over the 10.0 Giga bits per second data rates and spectral efficiencies of more than 120.0 bits per second to avoid the unnecessary delays in critical situations like bomb detection, material testing, patient report/state trans-communication etc.

Thz frequency range (0.1–10.0) can be fulfilled by using photonic band-gap structures (PBG) as one of the options. Graphene was used as a substrate due to its ability to control surface waves. The drawback of graphene antennas was that they suffer deterioration of radiation efficiency, but overall it has very high electrical conductivity, directivity, and miniaturized structure.

Earlier to fabricate antenna, copper was used but as it suffered degradation in radiation efficiency and propagation loss, it was replaced by copper nanotube (CNT) and graphenes. The reason for opting CNT and graphene is because, CNT has high conductivity and kinetic inductance as compared with copper, and graphene is used now-a-days because of its ability to support slow plasmonic rays at THz frequency. Therefore, graphene is preferred mostly upon CNT and copper. In THz frequency, copper's skin depth and conductivity decreases as increase in frequency.

Graphene was discovered by Novoselov et al. in 2004, is a 2D mono layer of sp^2 -bonded carbon atoms, having 1.42 nm spacing between two carbon atoms and 0.335 nm inter-planar spacing between two graphene sheets. The structure of the graphene is a honeycomb type lattice structure. It is a zero-overlap semiconductor having high electrical conductivity. Narrow strip of graphene sheet called GNR is of two kinds, armchair and zig-zag.

Armchair-shaped edges behave both either metallic or semi-conductor while zig-zag behave only metallic. Due to its property of propagating waves of surface plasmon polariton, it is laid in infinite thin sheet having complex surface conductivity. This conductivity can be both intraband and interband. However, intra-band dominates over interband in low THz frequency range. The CNT was discovered by Sumio Iijima in 1991, is nothing but rolled form of graphene sheets. They can be either single-walled or multi-walled. Single-walled can be zigzag which is an insulator, armchair, a conductor and chiral, semi-conductor. Power dissipation is low in CNT materials, leading to high antenna efficiency. The CNT also supports slow-wave propagation, enabling high miniaturization. Graphene is a planar structure while CNT and copper dipoles are cylindrical structures. At one THz frequency, length of graphene dipole antenna is 68.0 μm , copper dipole antenna's length is 139.0 μm and CNT antenna's length is 99.0 μm and directivities are 3.27, 2.26, and 3.02 dBi, respectively. The design is shown in Fig. 28 [139].

A design with graphene was used as a substrate to support highly-confined surface waves of lower wavelength. In a design, three patch antennas on three substrate materials i.e silica-oxide, epsilon-near-zero (ENZ) medium, and air were used. The dimensions of these three substrate materials were, 11.2 \times 5.6 mm², 24.0 \times 12.0 mm², and 48.7 \times 24.35 mm², respectively. The efficiency was 16.6% in the frequency band of 1.0–2.0 THz. The design is shown in Fig. 29 [140].

Similarly, the polyimide substrate with rectangular patch antenna and with circular cut from both broad sides was designed with photonic band gap (PBG) structures to resonate in 0.615–0.651 THz frequency band on 800.0 \times 600.0 \times 191.29 μm^3 polyimide substrate. The rectangular patch was cut in a curvature of radius 75.0 μm from both the sides. This cut in radius reduced the size of the antenna and the PBG structure resulted in high peak gain and efficiency. The gain and efficiency of the designed antenna were 7.934 dB and 85.93% respectively. The design is

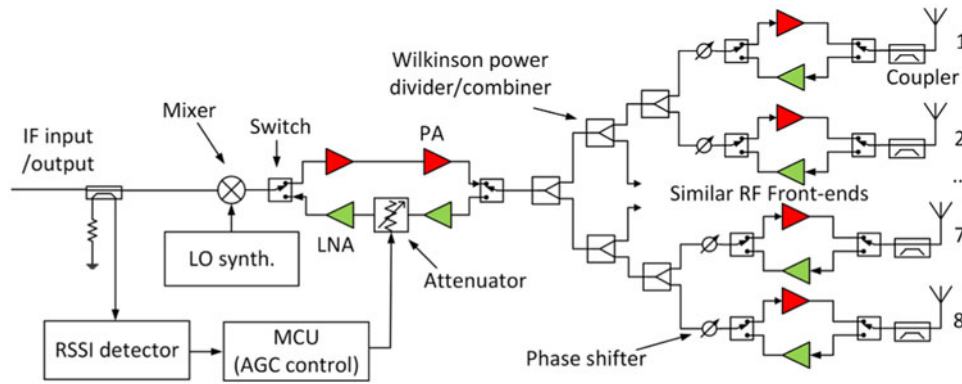


Fig. 27. Block diagram of transceiver at 28 GHz ©[138]

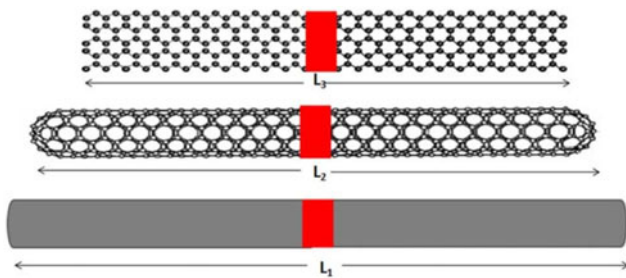


Fig. 28. Modeled THz copper, CNT and graphene dipoles of lengths L1, L2, and L3, respectively ©[139]

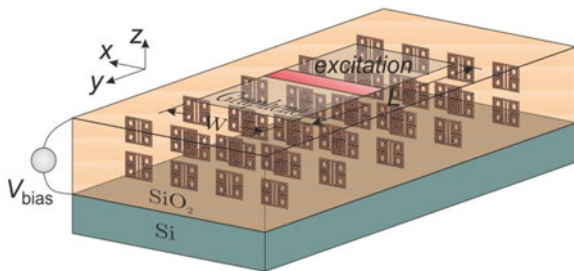


Fig. 29. Graphene plasmonic antenna ©[140]

shown in figure 30. The dimensions of rectangular patch antenna were calculated by equations (33) and (34) [141]:

$$W_p = \frac{2M + 1}{\epsilon_r} * \frac{\lambda_o}{2}, \tag{33}$$

$$L_p = \frac{2N + 1}{\sqrt{\epsilon_{eff}}} * \left(\frac{\lambda}{2}\right) - 2 * \Delta L, \tag{34}$$

where W_p and L_p were the width and length of patch respectively, M and N were non-negative integers, λ_o and λ were free space and operating wavelengths respectively, ΔL was patch length extension due to fringing field effect. The width of feed, W_f was calculated

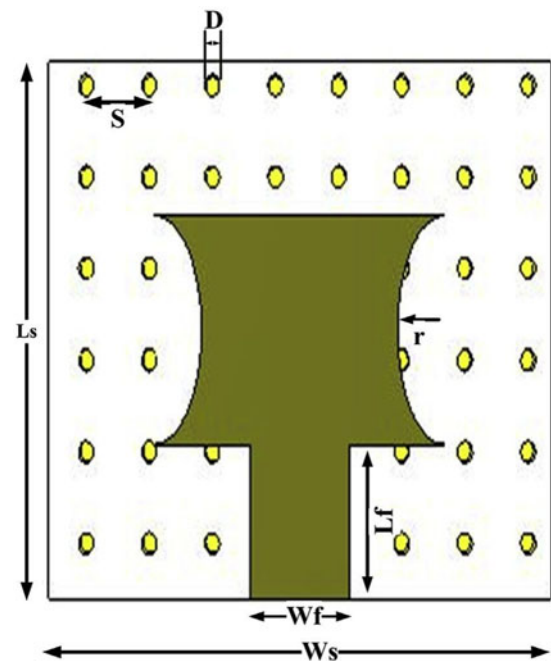


Fig. 30. THz antenna with PBG ©[141]

by equation (35):

$$W_f = \frac{7.475h}{\exp(x)} - 1.25t, \tag{35}$$

where t is patch thickness, and x is formulated by equation (36):

$$x = Z_o \frac{\sqrt{\epsilon_r + 1}}{87}. \tag{36}$$

The dimensions of substrate and ground were calculated by the formulas, having W_s , W_g , L_s and L_g as width and length of substrate and patch, respectively, by equations (37) and (38) as:

$$W_s = W_g = W_p + 2 * L_f, \tag{37}$$

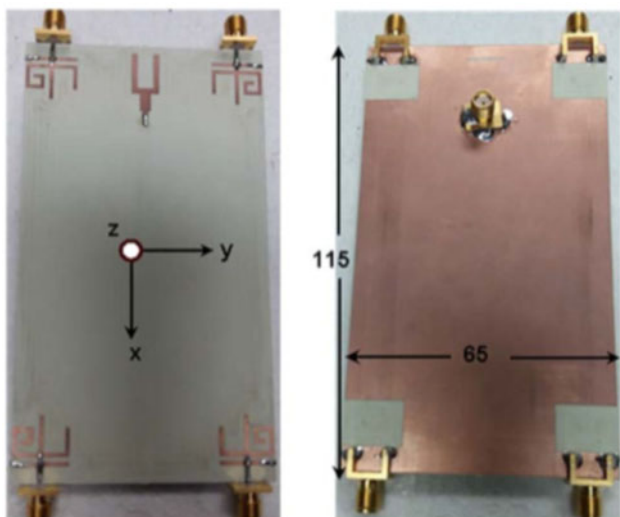


Fig. 31. CAA MIMO antenna array ©[143]

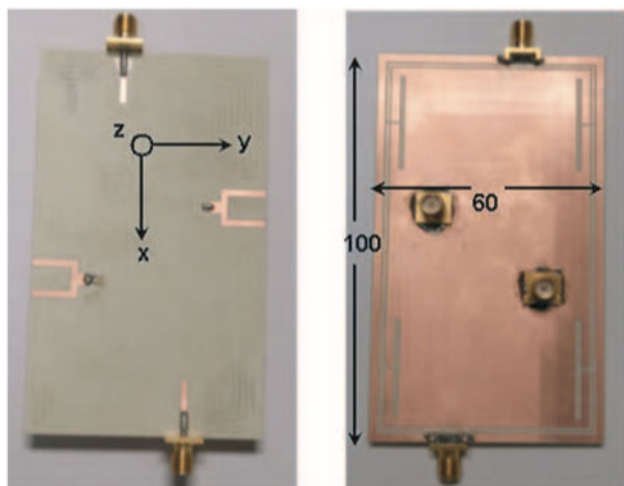


Fig. 32. Integrated design with isolation enhancement structure ©[144]

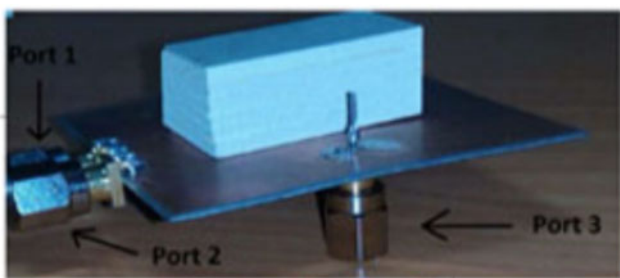


Fig. 33. Multi-mode MIMO DRA antenna ©[145]

$$L_s = L_g = L_p + 2 * L_f. \quad (38)$$

To use antennas in THz applications, graphene plasmonic antennas are attracting researchers and industrialists. Earlier, THz antennas were using copper, graphene, and carbon nanotubes, but since they did not meet all the requirements of THz

applications, surface plasmon polariton (SPP) was used so that applications and requirements of THz range can be fulfilled. The silicon-oxide material having dimension of $80.0 \times 15.0 \times 1.0 \text{ mm}^3$ was used as substrate. The frequency range lied between 0.1 and 10.0 THz [142].

4G and 5G combined antennas

Some of the designs are using the 4G and 5G combinations to accommodate both the generations of antennas. Few of the available designs are included in literature.

To cover bands of both 4G and 5G, a MIMO and connected antenna array (CAA) was combined. The CAA etched on ground plane was excited using slot and also uses 2×1 power divider/combiner arms. The lower bands of 4G antennas were covered using 4-element MIMO monopole antenna system while CAA slot covered 5G band. The gain and efficiency achieved on lower side were 5.0 dBi and 80.0%, respectively, while upper side achieved 9.65 dBi gain and 75.0% efficiency. The size of the antenna was $14.5 \times 11.0 \text{ mm}^2$, with isolation of $>13.0 \text{ dB}$, and ECC of <0.5 were achieved with this design. The size of substrate was $115.0 \times 65.0 \times 0.76 \text{ mm}^3$. The frequency bands covered 4G was from 1843.0 to 3305.0 MHz, while that of 5G was between 3500.0 and 3740.0 MHz. The design is shown in figure 31 [143].

A 4G/5G MIMO antenna system was made by integrating 2-element slots for 4G and 2-element MIMO-based connected array for 5G band. On the periphery of ground plane, two rectangular loops are etched. The thin loops on top and bottom act as 4G MIMO and parts of sides act as 5G arrays. The thickness of RO 4350 substrate material was 0.76 mm. The dimension of single antenna was $100.0 \times 60.0 \times 0.76 \text{ mm}^3$. For 4G, gain was 2.22 dBi, and for 5G gain was 8.0 dBi. Two resonant frequencies at 2.45 and 17.3 GHz were obtained with efficiencies as 27.0 and 80.0%, respectively. By implementing four narrow loops, isolation can be enhanced greatly in the band of 16.50–17.80 GHz. The value of ECC was <0.5 in the band. The design is shown in figure 32 [144].

The three-port MIMO DRA having three mutually decoupled modes was achieved by exciting two modes out of three and then overlapping the third perpendicular to their field magnitudes. The gain of 8.1, 7.4, and 7.5 dB was attained in the 8.6–10.2 GHz frequency range, having 720.0 MHz bandwidth. The antenna consisted of two parts, i.e rectangular DRA and feeding system. Rectangular DRA was fabricated on Rogers RT 6010 and feeding system which consisted of two microstrip lines having five identical apertures etched on ground plane. The feeding system placed on lower substrate was made of Rogers RT 5880 material. Overall dimensions of antenna and substrate were $56.6 \times 56.6 \times 14.09 \text{ mm}^3$ and $31.5 \times 17.8 \times 13.3 \text{ mm}^3$, respectively. In the desired bandwidth, ECC was <0.002 and isolation was 20.0 dB. The design is shown in figure 33 [145].

Finally, the 5G antennas have been summarized and compared in tables 2 and 3 on the basis of the frequencies used for 5G for single element/array/MIMO antenna. The other parameters compared in these tables are no. of radiating elements, size of the designed antenna, gain, efficiency, and isolation. Most of them are arrays and MIMO antennas. The designers/researchers used various bands for the 5G technology and ultimately, the goal is to make them compact, high gain for single and multi-element/port, and highly isolated in the case of multi-element/port antennas for different applications.

Table 2. Comparison of antennas having 28.0 GHz frequency range

Ref no.	Freq band/bands	No. of	Size	Gain	Efficiency	Isolation	Applications
[28]	27.2–29.0 GHz	–	0.20 mm ³	20.0 dBi	–	–	Wireless handheld devices
[29]	27.5–28.7 GHz	1	19.71 mm ²	–	–	–	Wireless handheld devices
[33]	22.0–35.0 GHz	4	128.44 mm ³	> 3.8 dBi	43.0%	–	5G Mobile transceivers
[37]	26.8–28.4 GHz	4	1.95 mm ³ (MIMO 1), 2.09 mm ³ (MIMO 2)	9.5–11.0 dBi	–	> 20.0 dB	Future wireless devices
[40]	26.9–29.21 GHz	40	5 cm ³	21.0 dBi	–	–	Future wireless devices
[43]	27.0–32.0 GHz	4	0.20 cm ³	16.3 dBi	71.8%	–	Laptop and portable devices
[44]	27.61–28.43 GHz	4,9	0.25 mm	7.73 dBi	88.0%	> 29.0 dB	Wireless handheld devices
[47]	27.9–28.5 GHz	1	–	> 6.0 dBi	–	–	Handheld devices
[49]	27.0–29.0 GHz	2	78.0 cm ²	23.3 dB	96.0%	–	Handheld devices
[61]	26.5–28.92 GHz	5	0.508 mm	13.5 dBi	–	–	Mobile communications
[65]	25.0–30.0 GHz	8	6.4558 cm ²	18.52 dBi	74.3, 68.0 and 72.2%	> 12.75 dB	MIMO synthetic aperture-radar-imagery applications
[70]	26.5–29.7 GHz	8	2.199 mm	14.9 dBi	75.0%	–	Mobile communications
[75]	22.0–32.0 GHz	12	1.27 cm ³	> 17.61 dB	> 92.2%	–	Mobile and wireless communications
[76]	27.0–29.0 GHz	–	0.127 mm	–	–	> 10.0 dB	Mobile applications
[79]	24.0–32.0 GHz	1, 2 and 4	1.18, 1.94 5.2 cm ³	7.13, 9.83 and 12.61 dBi	95.8%	–	Multi-beam massive MIMO communication
[83]	22.5–32.0 GHz	3	0.254 mm	8.2–9.6 dBi	–	–	Mobile and wireless communications
[87]	26.0–38.0 GHz	8	0.254 mm	11.5–12.5 dBi	> 93.0%	–	Future wireless communication systems
[90]	25.1–37.5 GHz	4	115.2 mm ³	10.6 dBi	> 80.0%	≤0.09 dB	Future 5G base station applications
[93]	24.55–28.5 GHz	8	1.361 cm ³	6.93–11.32 dBi	–	37.3 dB	MIMO antenna systems
[99]	27.528–63.0 GHz	8	2.20 mm ³	6.9 dBi	–	> 17.0 dB	Future wireless communication systems and networks
[103]	26.0–36.0 GHz	16	4 cm ²	3.8 dBi	–	–	Mobile handheld devices
[107]	26.0–30.5 GHz	2	0.52 cm ³	17.78 dBi	90.0%	–	Future mobile phone applications
[110]	23.5–33.11 GHz	12	976.6 mm ³	–	–	–	MIMO antenna systems
[131]	27.0–29.1 GHz	4	33.528 mm ³	12.1 dB	–	> 15.0 dB	Handset devices


Table 3. Comparison of antennas having 60.0 GHz frequency range

Ref no.	Freq band/bands	No. of elements	Size	Gain	Efficiency	Isolation	Applications
[34]	57.0–64.0 GHz	3	45.61 cm ³	20.0 dBi	83.0%	–	High data rate indoor communication
[36]	57.0–64.0 GHz	2	19.67 mm ³	10.0– 14.7 dBi	35.0– 40.0%	–	High data rate indoor communication
[41]	57.0–65.0 GHz	4	6.35 mm ³ and 4.06 cm ²	13.2, 10.3 dBi	–	–	Broadband MIMO communication systems
[48]	56.6–64.8 GHz	7	0.254 mm	7.9 dB	91.0%	46.5 dB	High data rate indoor communication
[55]	53.3–66.5 GHz	16	82.296 mm ³	> 12.0 dBi	–	–	High data rate wireless personal area network (WPAN)
[58]	55.4–66.6 GHz	16	67.66 mm ³ and 133.3 mm ³	16.8 dBi	> 90.0%	–	Short distance communication systems
[59]	57.0–63.0 GHz	16	182.67 mm ³	18.7, 18.6 and 18.8 dB	–	–	High data rate indoor communication

Conclusion

The 5G wireless network will specify the growth beyond mobile internet to massive IOT in the upcoming years. Main highlights compared with 4G/LTE is that besides data speed requirements, IOT and communication mechanisms will require new types of improved performances. Unlike IOT current services, 5G networks will be designed to bring the level of performance needed for massive IOT.

Different types of structures were investigated like PEG, PSG, SIW, corrugated structures, multiple notch, RRS, and PBG. Along with these structures, various kinds of antennas and arrays like patch/dipole/folded antennas, power divider arms-based arrays, combined antenna arrays, MIMO, etc on numerous kinds of substrates like FR-4, Taconic TLY-5, Rogers TMM4, Rogers 4003, Rogers 5800, etc have been studied and presented in this paper. The effects of stubs, slots, slits, parasitic element directors, baluns, CPW-fed with T-shaped element, etc have been presented with their impacts on the parameters of antenna. Thus, It has been observed that most of the structures provided higher than 80.0% efficiency, >10.0 dBi gain, and ECC of <0.01. The 5G can be considered as a boon to the market with its compact size and higher gain, high data rate, and battery life etc. The effect of beam steering with the transceiver showed the desired direction of radiation. Definitely, the higher capacity and accommodation of growing population can be done with the 5G and THz applications. Apart from 5G antennas some of the available THz antennas with different dielectric substrates have been discussed.

Author ORCID.  Leeladhar Malviya, 0000-0002-7342-4766

References

- Bliss DW and Govindasamy S (2013) *Adaptive Wireless Communications*, 1st Edn. UK: Cambridge University Press.
- Dahlman E, Parkvall S and Skold J (2013) *4G: LTE/LTE-Advanced for Mobile Broadband*, 2nd Edn. Sweden: Elsevier.
- Benson FA and Benson TM (1991) *Fields, Waves and Transmission Lines*. Netherlands: Springer.
- Kraus JD (1992) *Electromagnetics*, 4th Edn. New York: McGraw-Hill Companies.
- Jordan EC and Balmain KG (2011) *Electromagnetic Waves and Radiating Systems*, 2nd Edn. New Jersey, US: Pearson.
- Biglieri E, Calderbank R, Constantinides A, Goldsmith A, Paulraj A and Poor H (2010) *MIMO Wireless Communications*, 1st Edn. USA: Cambridge University Press.
- Hampton J (2013) *Introduction to MIMO Communications*, 1st Edn. New York: Cambridge University Press.
- Moradikordalivand A, Leow CY, Rahman TA, Ebrahimi S and Chua TH (2016) Wideband MIMO antenna system with dual polarization for WiFi and LTE applications. *International Journal of Microwave and Wireless Technologies* **8**, 643–650.
- Warren D and Dewar C (2014) Understanding 5G: perspectives on future technological advancements in mobile. *GSMA Intelligence*, 1–26.
- Boxall A and Jansen M (2019) Xiaomi Mi mix 3: everything you need to know, Digital Trends.
- Boxall A (2019) Samsung galaxy S10 5G phone: everything you need to know, Digital Trends.
- Li Y, Wang C, Yuan H, Liu N, Zhao H and Li X (2016) A 5G MIMO antenna manufactured by 3D printing method. *IEEE Microwave and Wireless Components Letters* **16**, 657–660.
- Rappaport T (1996) *Wireless Communications: Principles and Practice*, 2nd Edn. Upper Saddle River, NJ: Pearson.
- Schiller J (2003) *Mobile Communications*, 2nd Edn. UK: Pearson.
- Molisch AF (2010) *Wireless Communications*, 2nd Edn. UK: Wiley-IEEE Press.
- Garg V (2008) *Wireless Communications and Networking*, 1st Edn. San Francisco, US: Elsevier.
- Rodriguez J (2015) *Fundamentals of 5G Mobile Networks*. UK: Wiley.
- Osseiran A, Monserrat JF and Marsch P (2016) *5G Mobile and Wireless Communications Technology*. USA: Cambridge University Press.
- Yang Y, Chu Q and Mao C (2016) Multiband MIMO antenna for GSM, DCS and LTE indoor applications. *Antennas and Wireless Propagation Letters* **15**, 1573–1576.
- Kim S and Tentzeris MM (2018) Parylene coated waterproof washable inkjet-printed dual-band antenna on paper substrate. *International Journal of Microwave and Wireless Technologies* **10**, 1–5.
- Malviya L, Panigrahi RK and Kartikeyan MV (2016) A 2 × 2 dual-band MIMO antenna with polarization diversity for wireless applications. *Progress In Electromagnetic Research C* **61**, 91–103.
- Balanis CA (2016) *Antenna Theory: Analysis And design*, 4th Edn. New York: Wiley.
- Pozar DM (2013) *Microwave Engineering*, 4th Edn. US: Wiley.
- Streetman BG (2014) *Solid State Electronic Devices*, 7th Edn. Upper Saddle River, NJ, USA: Pearson.
- Stutzman WL (1981) *Antenna Theory and Design*, 3rd Edn. USA: John Wiley and Sons.
- Malviya L, Panigrahi RK and Kartikeyan MV (2017) MIMO antennas with diversity and mutual coupling reduction techniques: a review. *International Journal of Microwave and Wireless Technologies* **9**, 1763–1780.
- Talha MY, Babu MY and Aldhaheer RW (2016) Design of a compact MIMO antenna system with reduced mutual coupling. *International Journal of Microwave and Wireless Technologies* **8**, 117–124.
- Bang J and Choi J (2018) A SAR reduced mm-wave beam-steerable array antenna with dual-mode operation for fully metal-covered 5G cellular handsets. *IEEE Transactions on Antennas and Propagation Letters* **17**, 1118–1122.
- Li K, Shi Y and Liang CH (2016) Quad-element multi-band antenna array in the smart mobile phone for LTE MIMO operations. *Microwave and Optical Technology Letters* **58**, 2619–2626.
- Das G, Sharma A, Gangwar RK and Sharawi MS (2018) Compact back-to-back DRA-based four-port MIMO antenna system with bi-directional diversity. *Electronics Letters* **54**, 884–886.
- Das G, Sharma A and Gangwar RK (2017) Dual port aperture coupled MIMO cylindrical dielectric resonator antenna with high isolation for WiMAX application. *Wiley Online Library* **27**, 1–10.
- Zhang W, Weng Z and Wang L (2018) Design of a dual-band MIMO antenna for 5G smartphone application, International Workshop on Antenna Technology (iWAT).
- Sun L, Feng H, Li Y and Zhang Z (2018) Tightly arranged orthogonal mode antenna for 5G MIMO mobile terminal. *Wiley Online Library* **60**, 1751–1756.
- Trifi MAA, Sharawi MS and Shamim A (2018) Massive MIMO antenna system for 5G base stations with directive ports and switched beamsteering capabilities. *IET Microwaves, Antennas and Propagation* **12**, 1709–1708.
- Roslan SF, Kamarudin MR, Khalily M and Jamaluddin MH (2014) An MIMO rectangular dielectric resonator antenna for 4G applications. *IEEE Antennas and Wireless Propagation Letters* **13**, 321–324.
- Malviya L, Panigrahi RK and Kartikeyan MV (2015) Pattern diversity based MIMO antenna for low mutual coupling, IEEE Applied Electromagnetics Conference (AEMC), Guwahati.
- Sun K, Yang D and Liu S. (2018) A wideband hybrid feeding circularly polarized magneto-electric dipole antenna for 5G Wi-Fi. *Wiley Online Library* **60**, 1837–1842.
- Imran D, Farooqi MM, Khattak MI, Ullah Z, Khan MI, Khattak MA and Dar H (2018) Millimetre wave microstrip patch antenna for 5G mobile communication. *IEEE Transactions on Antennas and Propagation* **65**, 4864–4868.

39. Saxena S, Kanaujia BK, Dwari S, Kumar S and Tiwari R (2018) MIMO antenna with built-in circular shaped isolator for sub-6-GHz 5G applications. *Electronics Lett. Letters* **54**, 478–480.
40. Lim S, Choi WC and Yoon YJ (2015) Miniaturized radio frequency choke using modified stubs for high isolation in MIMO systems. *Journal of Electromagnetic Engineering and Science* **15**, 219–223.
41. Malviya L, Malik J, Panigrahi RK and Kartikeyan MV (2016) Circularly polarized 2×2 MIMO antenna for WLAN applications. *Progress In Electromagnetics Research C* **66**, 97–107.
42. Li G, Zhai H, Ma Z, Liang C, Yu R and Liu S (2014) Isolation-improved dual-band MIMO antenna array for LTE/WiMAX mobile terminals. *IEEE Antennas and Wireless Propagation Letters* **13**, 1128–1131.
43. Huang H, Li X and Liu Y (2018) 5G MIMO antenna based on vector synthetic mechanism. *IEEE Transactions on Antennas and Propagation Letters* **17**, 1052–1055.
44. Ardakani MD and Amiri R (2017) Mutual coupling reduction of closely spaced MIMO antenna using frequency selective surface based on meta-materials. *ACES Journal* **32**, 1064–1068.
45. Malviya L, Panigrahi RK and Kartikeyan MV (2018) Four element planar MIMO antenna design for long-term evolution operation. *IETE Journal of Research* **64**, 367–373.
46. Sarkar D and Srivastava KV (2017) Compact four-element SRR-loaded dual-band MIMO antenna for WLAN/WiMAX/WiFi/4G-LTE and 5G applications. *Electronics Lett. Letters* **53**, 1623–1624.
47. Li H, Kang L, Xu Y and Yin YZ (2016) Planar dual-band WLAN MIMO antenna with high isolation. *ACES Journal* **31**, 1410–1415.
48. Paulraj A and Kailath T (Increasing capacity in wireless broadcast systems using distributed transmission/directional reception, U.S. Patent 1994:5345599.
49. Hu HT, Chen FC and Chu QX (2016) A compact directional slot antenna and its application in MIMO array. *IEEE Antennas and Propagation* **64**, 5513–5517.
50. Guan TM and Rahim SKA (2017) Compact monopole MIMO antenna for 5G application. *Microwave and Optical Technology Letters* **59**, 1074–1077.
51. Malviya L, Panigrahi RK and Kartikeyan MV (2016) Proximity coupled MIMO antenna for WLAN/WiMAX applications, Proceedings of the Asia-Pacific Microwave Conference.
52. Li L, Huo F, Jia Z and Han W (2013) Dual zeroth-order resonance antennas with low mutual coupling for MIMO communications. *IEEE Antennas and Wireless Propagation Letters* **12**, 1692–1695.
53. Wang K, Mauermayer RAM and Eibert TF (2015) Contour-integrated dual-band compact antenna elements and arrays for low-profile mobile terminals. *IEEE Transactions on Antennas and Propagation* **63**, 3305–3311.
54. Malviya L, Panigrahi RK and Kartikeyan MV (2018) Multi-standard, multi-band planar multiple input multiple output antenna with diversity effects for wireless applications. *International Journal of Wiley RF and Microwave Computer-Aided Engineering* **29**, 1–8.
55. Shoaib S, Shoaib I, Shoaib N, Chen X and Parini CG (2017) Design and performance study of a dual-element multiband printed monopole antenna array for MIMO terminals. *IEEE Antennas and Wireless Propagation Letters* **13**, 329–332.
56. Malviya L, Panigrahi RK and Kartikeyan MV (2016) A multi-standard, wide-band 2×2 compact MIMO antenna with ground modification techniques. *International Journal of Microwave and Optical Technology* **11**, 259–267.
57. An W, Li Y, Fu H, Ma J, Chen W and Feng B (2018) Low-profile and wideband microstrip antenna with stable gain for 5G wireless applications. *IEEE Transactions on Antennas and Wireless Propagation Letters* **17**, 621–624.
58. Toktas A and Akdagli A (2014) Wideband MIMO antenna with enhanced isolation for LTE, WiMAX and WLAN mobile handsets. *Electronics Lett. Letters* **50**, 723–724.
59. Chen YS and Chang CP (2016) Design of a four-element multiple-input-multiple-output antenna for compact long-term evolution small-cell base stations. *IET Microwaves, Antennas and Propagation* **10**, 385–392.
60. Hakanoglu BG and Turkmen M (2017) An inset fed square microstrip patch antenna to improve the return loss characteristics for 5G applications, 32nd URSI GASS Montreal.
61. Yang B, Yu Z, Zhou J and Hong W (2017) Compact tapered slot antenna array for 5G millimeter-wave massive MIMO systems. *IEEE Transactions on Antennas and Propag.* **65**, 6721–6727.
62. Minasian AA and Bird TS (2013) Particle swarm optimization of microstrip antennas for wireless communication systems. *IEEE Transactions on Antennas and Propagation* **61**, 6214–6217.
63. Gao Y, Ma R, Wang Y, Zhang Q and Parini C (2016) Stacked patch antenna with dual-polarization and low mutual coupling for massive MIMO. *IEEE Transactions on Antennas and Propagation* **64**, 4544–4549.
64. Li MY, Ban YL, Xu ZQ, Wu G, Sim CYD, Kang K and Yu ZF (2016) Eight-pot orthogonally dual-polarized antenna array for 5G smartphone applications. *IEEE Transactions on Antennas and Propagation* **64**, 3820–3830.
65. Komandla MV, Mishra G and Sharma SK (2017) Investigations on dual slant polarized cavity backed massive MIMO antenna panel with beamforming. *IEEE Transactions on Antennas and Propagation* **65**, 6794–6799.
66. Malviya L, Panigrahi RK and Kartikeyan MV (2017) A low profile MIMO antenna with polarization diversity for 1800/1900 applications. *Microwave and Optical Technology Letters* **59**, 533–538.
67. Malviya L, Panigrahi RK and Kartikeyan MV (2016) 2×2 MIMO antenna for ISM band application, 11th International Conference on Industrial and Information Systems (ICIIS).
68. Malviya L, Panigrahi RK and Kartikeyan MV (2015) Design of a compact MIMO antenna with polarization diversity technique for wireless communication, International Conference on Microwave Optical and Communication Engineering. pp. 21–24.
69. Luk KM and Leung KW (2002) *Dielectric Resonator Antennas*. Baldock, U.K.: Research Studies Press.
70. Mak KM, Lai HW and Luk KM (2018) A 5G wideband patch antenna with antisymmetric L-shaped probe feeds. *IEEE Transactions on Antennas and Propagation* **65**, 957–961.
71. Ge X, Yang J, Gharavi H and Sun Y (2017) Energy efficiency challenges of 5G small cell networks. *IEEE Communications Magazine* **55**, 184–191.
72. Choudhary P, Kumar R and Gupta N (2015) Dielectric material selection of microstrip patch antenna for wireless communication applications using Ashby's approach. *International Journal of Microwave and Wireless Technologies* **7**, 579–587.
73. Sima W, Jiang X, Peng Q and Sun P (2017) Investigation of dielectric properties of polyethylene terephthalate under different aging temperatures. *IEEE Transactions on Dielectrics and Electrical Insulation* **24**, 3015–3023.
74. Muhamad WAW, Ngah R, Jamlos MF, Soh PJ and Ali MT (2017) High gain dipole antenna using polydimethylsiloxane-glass microsphere (PDMS-GM) substrate for 5G application. *Applied Physics A: Material Science and Processing* **123**, 101–105.
75. Tighezza M, Rahim SKA and Islam MT (2018) Flexible wideband antenna for 5G applications. *IEEE Transactions on Antennas and Propagation* **60**, 38–44.
76. Kong L and Xu X (2018) A compact dual-band dual-polarized microstrip antenna array for MIMO-SAR applications. *IEEE Transactions on Antennas and Propagation* **66**, 2374–2381.
77. Honari MM, Mirzavand R, Melzer J and Mousavi P (2016) A new aperture antenna using substrate integrated waveguide corrugated structures for 5G applications. *IEEE Antennas and Wireless Propagation Letters* **16**, 254–257.
78. Ramli MR, Rahim SKA, Rahman HA, Sabran MI and Samingan ML (2017) Flexible microstrip grid array polymer-conductive rubber antenna for 5G mobile communication application. *Wiley Online Library* **59**, 1866–1870.
79. Shahadan NH, Jamaluddin MH, Kamarudin MR, Yamada Y, Khalily M, Jusoh M and Dahlan SH (2017) Steerable higher order mode dielectric resonator antenna with parasitic elements for 5G applications. *IEEE Access* **5**, 22234–22243.
80. Yahya MS and Rahim SKA (2016) 15 GHz grid array antenna 5G mobile communications system. *Microwave and Optical Technology Letters* **58**, 2977–2980.

81. **Zhao K, Ying Z and He S** (2015) EMF exposure study concerning mmWave phased array in mobile devices for 5G communication. *IEEE Antennas and Wireless Propagation Letters* **15**, 1132–1135.
82. **Ojaroudiparchin N, Shen M, Zhang S and Pedersen GF** (2016) A switchable 3D-coverage phased array antenna package for 5G mobile terminals. *IEEE Antennas and Wireless Propagation Letters* **15**, 1747–1750.
83. **Parchin NO, Shen M and Pedersen GF** (2017) Small-size tapered slot antenna (TSA) design for use in 5G phased array applications. *ACES Journal* **32**, 193–202.
84. **Ojaroudiparchin N, Shen M and Pedersen GF** (2016) Investigation on the performance of low-profile insensitive antenna with improved radiation characteristics of the future 5G applications. *Microwave and Optical Technology Letters* **58**, 2148–2151.
85. **Mao CX, Gao S and Wang Y** (2018) Broadband high-gain beam-scanning antenna array for millimetre-wave applications. *IEEE Transactions on Antennas and Propagation* **65**, 4864–4868.
86. **Malviya L, Panigrahi RK and Kartikeyan MV** (2018) Offset planar MIMO antenna for omnidirectional radiation patterns. *International Journal of RF and Microwave Computer-Aided Engineering* **28**, 1–9.
87. **Afoakwa S and Jung YB** (2017) Wideband microstrip comb-line linear array antenna using stubbed-element technique for high sidelobe suppression. *IEEE Transactions on Antennas and Propagation* **65**, 5190–5199.
88. **Halwagy WE, Mirzavand R, Melzer J, Hossain M and Mousavi P** (2017) Investigation of wideband substrate-integrated vertically-polarized electric dipole antenna and arrays for mm-Wave 5G mobile devices. *IEEE Access* **6**, 2145–2157.
89. **Zhu S, Liu H, Wen P and Chen Z** (2018) A compact gain-enhanced vivaldi antenna array with suppressed mutual coupling for 5G mm wave application. *IEEE Transactions on Antennas and Wireless Propagation Letters* **17**, 776–779.
90. **Zhang S, Chen X, Syrtytsin I and Pedersen GF** (2017) A planar switchable 3-D coverage phased array antenna and its user effects for 28 GHz mobile terminal applications. *IEEE Transactions on Antennas and Propagation* **65**, 6413–6421.
91. **Ta SX, Choo H and Park I** (2017) Broadband printed-dipole antenna and its arrays for 5G applications. *IEEE Antennas and Wireless Propagation Letters* **16**, 2183–2186.
92. **Jilani SF and Alomainy A** (2018) Millimetre-wave T-shaped MIMO antenna with defected ground structures for 5G cellular networks. *IET Microwave Antennas Propagation* **12**, 672–677.
93. **Asaadi M, Affi I and Sebak A** (2018) High gain and wideband high dense dielectric patch antenna using FSS superstrate for millimeter-wave applications. *IEEE Access* **6**, 38243–38250.
94. **Liu D, Gu X, Baks CW and Garcia AV** (2017) Antenna-in-package design considerations for Ka-band 5G communication applications. *IEEE Transactions on Antennas and Propagation* **65**, 6372–6379.
95. **Wang Y and Du Z** (2015) Dual-polarized slot-coupled microstrip antenna array with stable active element pattern. *IEEE Transactions on Antennas and Propagation* **63**, 4239–4244.
96. **Lin W, Ziolkowski RW and Baum TC** (2017) 28 GHz compact omnidirectional circularly polarized antenna for device-to device communications in the future 5G systems. *IEEE Transactions on Antennas and Propagation* **65**, 6904–6914.
97. **Park SJ, Shin DH and Park SO** (2016) Low side-lobe substrate-integrated-waveguide antenna array using broadband unequal feeding network for mm-wave handset device. *IEEE Transactions on Antennas and Propagation* **65**, 923–932.
98. **Diawuo HA and Jung YB** (2017) Wideband proximity coupled microstrip linear array design for 5G mobile communication. *Wiley Online Library* **59**, 2996–3002.
99. **Lin M, Liu P and Guo Z** (2017) Gain-enhanced Ka-band MIMO antennas based on the SIW corrugated technique. *IEEE Antennas and Wireless Propagation Letters* **16**, 3084–3087.
100. **Diawuo HA, Jung YB and Jung YB** (2018) Broadband proximity coupled microstrip planar antenna array for 5G cellular applications. *IEEE Transactions on Antennas and Wireless Propagation Letters* **17**, 1286–1290.
101. **Park SJ and Park SO** (2017) LHCP and RHCP substrate integrated waveguide antenna arrays for millimetre-wave applications. *IEEE Antennas and Wireless Propagation Letters* **16**, 601–604.
102. **Abbas EA, Abbosh AM and Bialkowski K** (2017) Tunable in-phase power divider for 5G cellular networks. *IEEE Microwave and Wireless Components Letters* **27**, 551–553.
103. **Nor NM, Jamaluddin MH, Kamarudin MR and Khalily M** (2016) Rectangular dielectric resonator antenna array for 28 GHz applications. *Progress In Electromagnetics Research C* **63**, 53–61.
104. **Haraz OM, Elboushi A, Alshebeili SA and Sebak AR** (2014) Dense dielectric patch array antenna with improved radiation characteristics using EBG ground structure and dielectric superstrate for future 5G cellular networks. *IEEE Access* **2**, 909–913.
105. **Luo J, He J, Wang H, Chang S, Huang Q and Yu XP** (2018) A 28 GHz LNA using defected ground structure for 5G application. *Wiley Online Library* **60**, 1067–1072.
106. **Yu B, Yang K, Sim CYD and Yang G** (2018) A novel 28 GHz beam steering array for 5G mobile device with metallic casing application. *IEEE Transactions on Antennas and Propagation* **66**, 462–466.
107. **Khalily M, Rahman TA and Kamarudin MR** (2015) Design of phased arrays of series-fed patch antennas with reduced number of the controllers for 28-GHz mm-wave applications. *IEEE Antennas and Wireless Propagation Letters* **15**, 1305–1308.
108. **Yashchyshyn Y, Derzakowski K, Bogdan G, Godziszewski K, Nyzovets D, Kim CH and Park B** (2018) 28 GHz switched-beam antenna based on S-PIN diodes for 5G mobile communications. *IEEE Antennas and Wireless Propagation Letters* **17**, 225–228.
109. **Kim E, Ko ST, Lee Y and Oh J** (2018) Millimeter wave tiny lens antenna employing U-shaped filter arrays for 5G. *IEEE Transactions on Antennas and Propagation* **17**, 845–848.
110. **Maina I, Rahman TA and Khalily M** (2015) Bandwidth enhanced and sidelobes level reduced radial line slot array antenna at 28 GHz for 5G next generation mobile communication. *ARPN Journal of Engineering and Applied Sciences* **10**, 5752–5757.
111. **Mahmoud KR and Montaser AM** (2017) Optimised 4 × 4 millimetre-wave antenna array with DGS using hybrid ECFO-NM algorithm for 5G mobile networks. *IET Microwaves, Antennas and Propagation* **11**, 1516–1523.
112. **Jilani SF and Alomainy A** (2017) A multiband millimeter-wave 2-D array based on enhanced franklin antenna for 5G wireless systems. *IEEE Antennas and Wireless Propagation Letters* **16**, 2983–2986.
113. **Mahmoud KR and Montaser AM** (2018) Design of dual-band circularly polarised array antenna package for 5G mobile terminals with beam-steering capabilities. *IET Microwaves, Antennas and Propagation* **12**, 29–39.
114. **Dadgarpour A, Sorkherizi MS and Kishk AA** (2017) High efficient circularly polarized magneto-electric dipole antenna for 5G applications using dual-polarized split-ring resonator lens. *IEEE Transactions on Antennas and Propagation* **65**, 4263–4267.
115. **Peristerianos A, Theopoulos A, Koutinos AG, Kaifas T and Siakavara K** (2016) Dual-band fractal semi-printed element antenna arrays for MIMO applications. *IEEE Antennas and Wireless Propagation Letters* **15**, 730–733.
116. **Chu QX, Li XR and Ye M** (2017) High gain printed log-periodic dipole array antenna with parasitic cell for 5G communication. *IEEE Transactions on Antennas and Propagation* **65**, 6338–6344.
117. **Zhu Q, Ng KB, Chou CH and Luk KM** (2017) Substrate-integrated-waveguide-fed array antenna covering 57–71 GHz band for 5G applications. *IEEE Transactions on Antennas and Propagation* **65**, 6298–6306.
118. **Lee B and Yoon Y** (2017) Low profile, low cost, broadband millimeter-wave antenna array for high data rate WPAN systems. *IEEE Antennas and Wireless Propagation Letters* **16**, 1957–1960.
119. **Attia H, Abdelghani ML and Denidni TA** (2017) Wideband and high-gain millimeter-wave antenna based on FSS fabry-perot cavity. *IEEE Transactions on Antennas and Propagation* **65**, 5589–5594.

120. **Dadgarpour A, Zarghooni B, Virdee BS, Denidni TA and Kishk AA** (2016) Mutual coupling reduction in dielectric resonator antennas using metasurface shield for 60 GHz MIMO systems. *IEEE Antennas and Wireless Propagation Letters* **16**, 477–480.
121. **Semkin V, Ferrero F, Bisogni A, Laurinaho JA, Luxey C, Devillers F and Raisanen AV** (2015) Beam switching conformal antenna array for mm-wave communications. *IEEE Antennas and Wireless Propagation Letters* **15**, 28–31.
122. **Briqech Z, Sebak AR and Denidni TA** (2016) Wide-scan MSC-AFTSA array-fed grooved spherical lens antenna for millimeter-wave MIMO applications. *IEEE Transactions on Antennas and Propagation* **64**, 2971–2980.
123. **Li Y, Wang J and Luk KM** (2017) Millimeter-wave multi-beam aperture-coupled magneto-electric dipole array with planar substrate integrated beam-forming network for 5G applications. *IEEE Antennas and Propagation* **65**, 6422–6431.
124. **Biglarbegian B, Fakharzadeh M, Busuioc D, Ahmadi MRN and Naeini SS** (2011) Optimized microstrip antenna arrays for emerging millimeter-wave wireless applications. *IEEE Transactions on Antennas and Propagation* **59**, 1742–1747.
125. **Yao Y, Cheng X, Wang C, Yu J and Chen X** (2017) Wideband circularly polarized antipodal curvedly tapered slot antenna array for 5G applications. *IEEE Journal on Selected Areas in Communications* **35**, 1539–1549.
126. **Uchendu I and Kelly JR** (2016) Survey of beam steering techniques available for millimeter wave applications. *Progress in Electromagnetics Research B* **68**, 35–54.
127. **Costas JP** (1981) An antenna beam steering technique comprised of constant-phase array elements. *Proceedings of the IEEE* **69**, 745–747.
128. **Thiel DV, O'Keefe S and Lu JW** (1996) Electronic beam steering in wire and patch antenna systems using switched parasitic elements. *IEEE Antennas and Propagation Society International Symposium* **1**, 534–537.
129. **Katare KK, Biswas A and Akhtar MJ** (2018) ESPAR-inspired mechanical beam steering antenna with high gain and wide bandwidth performance. *International Journal of RF and Microwave Computer-Aided Engineering* **60**, 1803–1808.
130. **Kojima N, Shiramatsu K, Chiba I, Ebisui T and Kurihara N** (1996) Measurement and evaluation techniques for an airborne active phased array antenna. *Phased Array Systems and Technology* 231–236.
131. **Yan S and Chu T** (2009) A beam-steering and-switching antenna array using a coupled phase-locked loop array. *IEEE Transactions on Antennas and Propagation* **57**, 638–644.
132. **Jung Y, Shishlov AV and Park S** (2009) Cassegrain antenna with hybrid beam steering scheme for mobile satellite communications. *IEEE Transactions on Antennas and Propagation* **57**, 1367–1372.
133. **Nassar MA, Soliman HY, Ghoneim A and Abuelenin A** (2017) Beam steering antenna arrays for 28-GHz applications, Loughborough Antennas and Propagation Conference (LAPC 2017), Loughborough, pp. 1–4.
134. **Ali E, Ismail M, Nordin R and Abdulah NF** (2017) Beamforming techniques for massive MIMO systems in 5G: overview, classification, and trends for future research. *IEEE Antennas and Wireless Propagation Letters* **18**, 753–772.
135. **Hwang RB, Tsai YC and Hsiao CC** (2015) An adaptive multi-beam massive array architecture for 5G wireless, IEEE International Symposium on Antennas and Propagation and USNC/URSI National Radio Science Meeting, Vancouver, BC, pp. 125–126.
136. **Liu C, Xiao S, Guo YX, Bai YY and Wang BZ** (2013) Broadband circularly polarized beam-steering antenna array. *IEEE Transactions on Antennas and Propagation* **61**, 1475–1479.
137. **Liu C, Xiao S, Guo YX, Tang MC, Bai YY and Wang BZ** (2011) Circularly polarized beam-steering antenna array with butler matrix network. *IEEE Antennas and Wireless Propagation Letters* **10**, 1278–1281.
138. **Kim HT, Park BS, Oh SM, Song SS, Kim JM, Kim SH, Moon TS, Kim SY, Chang JY, Kim SW, Kang WS, Jung SY, Tak GY, Du JK, Suh YS and Ho YC** (2017) A 28 GHz CMOS direct conversion transceiver with packaged antenna arrays for 5G cellular system, IEEE Radio Frequency Integrated Circuits Symposium (RFIC).
139. **Dash S and Patnaik A** (2018) Material selection for THz antennas. *Microwave and Optical Technology Letters* **60**, 1183–1187.
140. **Amanatiadis SA, Karamanos TD and Kantartzis NV** (2017) Radiation efficiency enhancement of graphene THz antennas utilizing metamaterial substrates. *IEEE Antennas and Wireless Propagation Letters* **16**, 2054–2057.
141. **Kushwaha RK, Karuppanan P and Malviya L** (2018) Design and analysis of novel microstrip patch antenna on photonic crystal in THz. *Physica B: Condensed Matter* **545**, 107–112.
142. **Dash S and Patnaik A** (2018) Performance of graphene plasmonic antenna in comparison with their counterparts for low-terahertz applications, Research Gate.
143. **Ikram M, Sharawi MS and Shamim A** (2017) A novel very wideband integrated antenna system for 4G and 5G mm-wave applications. *Wiley Online Library* **59**, 3082–3088.
144. **Sharawi MS, Ikram M and Shamim A** (2017) A two concentric slot loop based connected array MIMO antenna system for 4G/5G terminals. *IEEE Transactions on Antennas and Propagation* **65**, 6679–6686.
145. **Abdalrazik A, Hameed ASAE and Rahman AB** (2017) A three-port MIMO dielectric resonator antenna using decoupled modes. *IEEE Antennas and Wireless Propagation Letters* **16**, 3104–3017.



Parul Gupta is currently pursuing her ME in Electronics and Telecommunication Engineering from Shri G. S. Institute of Technology and Science, Indore (MP), India, in session 2017-19, and procured her BE in Electronics and Communication, from Indore Institute of Science and Technology, Indore (MP), India, in 2017. Her current research interests include compact multiple-input-multiple-output (MIMO) antennas for high data rate communications for 5G and planar microstrip antennas.



Leeladhar Malviya received his Ph.D. from IIT Roorkee, India in 2017. He received his ME in Electronics and Telecommunication Engineering from Shri G. S. Institute of Technology and Science, Indore (MP), India, in 2008, and BE in Electronics and Communication, from the Govt. Engineering College, Ujjain (MP), India, in 1998. Since 2001, he has been with Shri G. S. Institute of Technology and Science, Indore (MP), India, and serving as an Associate Professor. His current research interests include compact multiple-input-multiple-output (MIMO) antennas for high data rate communications for 4G, 5G, and THz planar microstrip antennas, fractal antennas, and metamaterial antennas for communication. He is a Member of IEEE, Institution of Electronics and Telecommunications Engineers (IETE, India) Institution of Engineers (IE, India), and Indian Society for Technical Education (ISTE).



Prof. S. V. Charhate is currently working in Shri G. S. Institute of Technology and Science since 1985. She received her ME in Computer Science Engineering from DAVV University, Indore (MP), India, in 1991, and BE in Electronics and Communication, from the Pune University, India, in 1981. She is a Member of Institution of Engineers (IE, India).